Lower-thermospheric winds at high latitude : Chatanika radar observations

R. M. JOHNSON (*) ([1, 2]), V. B. WICKWAR ([3]),
R. G. ROBLE ([4]), J. G. LUHMANN ([1])

([1]) *Institute of Geophysics and Planetary Physics, University of California at Los Angeles, Los Angeles, CA* 90024, *USA*
([2]) *Department of Earth and Space Sciences, University of California at Los Angeles, Los Angeles, CA* 90024, *USA*
([3]) *SRI International, 333 Ravenswood Avenue, Menlo Park, CA* 94025, *USA*
([4]) *High Altitude Observatory, National Center for Atmospheric Research* (**), *Boulder, CO* 80307, *USA*

Received April 15, 1987 ; revised July 17, 1987 ; accepted July 29, 1987.

ABSTRACT. Observations made of the high-latitude *E*-region with the Chatanika, Alaska (65° N), incoherent scatter radar facility during the summer months of 1976 to 1982 are presented. Fourteen 24-h experiments were performed with altitude resolution between 9 and 24 km. Ion drifts measured during these experiments have been analysed to obtain neutral winds at lower-thermospheric heights. Tidal oscillations are the predominant feature of the neutral winds from 90 to 125 km. The semidiurnal oscillation is particularly strong, attaining peak amplitudes of ≈ 50 m/s at 110 km. Average diurnal and semidiurnal tidal phases are in good agreement with previous mid- to high-latitude observations. Average neutral winds are determined for three different levels of geomagnetic activity. During geomagnetically active experiments, the average neutral wind circulation pattern was altered from its normal quiet-time behavior above 100 km. The changes observed in the neutral winds are generally consistent with the predictions of the National Center for Atmospheric Research (NCAR) Thermospheric General Circulation Model (TGCM) for three different levels of steady-state magnetospheric input that reflect increasing levels of geomagnetic activity.

Key words : lower thermosphere, tides, geomagnetic activity, high latitude.

Annales Geophysicae, 1987, **5A**, (6), 383-404.

INTRODUCTION

The lower thermosphere (90 to 130 km altitude range) is a region subjected to influences from both the upper and the lower atmosphere. Upwardly propagating diurnal and semidiurnal atmospheric tides, forced by insolation absorption by H_2O and O_3 in the lower atmosphere, are important particularly at low- to mid-latitudes. At high latitudes, although the lower-atmospheric diurnal tide is evanescent, the semidiurnal tide propagates upward and is a predominant feature. In addition, tides are forced *in situ* in the lower thermosphere through UV and EUV absorption. At high-latitudes, the energy and momentum source provided by magnetospheric forcing of the ionosphere-thermosphere system allows a mechanism by which lower-thermospheric neutral winds may be disturbed. It is particularly important for the development of realistic thermospheric general circulation models to obtain estimates of tidal components at lower-thermospheric heights, as well as to ascertain the extent to which ion drag and Joule heating associated with magnetospheric forcing are observed to alter lower-thermospheric neutral winds. The investigation described here focuses on the determination of the contributions that tidal and magnetospheric sources make to the dynamics of the high-latitude lower thermosphere.

Previous wind observations at these heights have been made mainly at low- to mid-latitude stations (see review articles by Evans, 1978 ; Forbes, 1985 ; also in order of increasing latitude, Mathews, 1976 ; Mathews *et al.*, 1981 ; Harper, 1981 ; Massebeuf *et al.*, 1981 ; Aso *et al.*, 1980 ; Vincent and Stubbs, 1977 ; Amayenc and Reddy, 1972 ; Bernard, 1974*a*, *b* ; Amayenc, 1974 ; Glass and Spizzichino, 1974 ; Fellous *et al.*, 1975 ; Wand, 1983*a*, *b* ; Manson *et al.*, 1974, 1979, 1981*a*, *b* ; Stening *et al.*, 1978 ; Müller, 1966). These studies, using incoherent scatter, meteor or partial reflection radars, have concentrated on under-

(*) Now at SRI International, U.S.A.

(**) The National Center for Atmospheric Research is sponsored by the National Science Foundation.

standing tidal fluctuations and mean flows in the lower thermosphere.

In addition, there have been many studies of neutral winds in the lower thermosphere using rocket chemical release techniques (see, for instance, Rees, 1972, 1979 ; Rees *et al.*, 1981 ; Pereira *et al.*, 1980 ; Heppner and Miller, 1982 ; Mikkelsen *et al.*, 1981). These studies have the drawback that chemical release studies obtain measurements from clouds drifting with the background wind field for several hours at most, and as such cannot provide an understanding of the variation at any one height over time. To attribute features observed in a rocket experiment to the influence of magnetospheric forcing is difficult unless an understanding of the normal variations observed at these heights has been previously obtained. Optical observations have provided useful information on lower-thermospheric winds and their variation with geomagnetic activity (Cogger *et al.*, 1985 ; Sica *et al.*, 1986) ; however, it is difficult to discern altitude structures and tides using this technique since the altitude of the emitting layer is not fixed and the emission generally occurs over a broad altitude region.

There have been only limited studies of lower-thermospheric neutral winds at high-latitude. Hook (1970) presented meteor wind observations obtained at College, Alaska (65° N), from 1966 to 1968 covering the 75 to 110 km altitude range. Several campaign length studies were carried out with the Kiruna, Sweden (68° N), meteor radar facility (Glass *et al.*, 1978). The Poker Flat, Alaska (65° N), Mesosphere-Stratosphere-Troposphere (MST) radar has provided a valuable long time-scale data base of upper-mesospheric neutral wind observations, spanning the 80 to 95 km regime (Carter and Balsley, 1982). However, the MST technique is not applicable in the lower thermosphere. Most recently, Tetenbaum *et al.* (1986) have reported on mean winds and tides in the 75 to 105 km altitude range observed during the 1980-1984 interval using meteor echoes obtained with the Poker Flat, MST radar. In addition, partial reflection measurements from Saskatoon (52° N) have been valuable in the study of mean winds and tidal structures in the upper mesosphere and lower thermosphere at moderately high latitudes (Manson *et al.*, 1974 ; 1979 ; 1981*a*, *b* ; Stening *et al.*, 1978).

The Chatanika, Alaska (65° N) incoherent scatter radar, which operated from 1971 to 1982, carried out experiments in several different modes with varying degrees of altitude resolution. Several studies of lower-thermospheric neutral winds were carried out using measurements obtained with a range resolution of approximately 50 km (Brekke *et al.*, 1973, 1974 ; Comfort *et al.*, 1976). From 1974 to 1982, the addition of an improved autocorrelator using the multipulse technique allowed better *E*-region altitude resolution to be obtained (Rino *et al.*, 1977). All of these studies focused on the relationship of the observed lower-thermospheric neutral wind field with the level of geomagnetic activity, with sometimes conflicting results. Although the presence and importance of tidal oscillations at *E*-region heights was recognized (Brekke *et al.*, 1973), no attempt was made to study them. In addition, no attempt was made to separate the changes attributed to magnetospheric effects from the normal variation in neutral winds over the period of the day due to the tides. However, in a study of *E*-region neutral temperature measurements obtained at Chatanika, Lathulliere *et al.* (1983) detected a systematic temperature difference between evening and morning hours, and proposed that it was of tidal origin. To date, there has been no study of tidal oscillations using Chatanika lower-thermospheric neutral winds.

From 1976 to 1982, 56 24-h experiments were performed with *E*-region altitude resolution ranging between 9 and 24 km, and a typical time resolution of 5 min per fixed position measurement. In the study described here, the summer experiments available in the Chatanika library of observations have been analysed. This more than doubles the number of day-long *E*-region experiments at Chatanika reported in the literature, and is the first study of neutral dynamics in the high-latitude *E*-region using a large data set with relatively high altitude resolution.

DATA ANALYSIS

Autocorrelation functions of the return signal are calculated for several different range gates at *E*- and *F*-region heights. These measured functions are then fit in a nonlinear least-squares sense to theoretical autocorrelation functions to obtain values and uncertainties for the important geophysical parameters, including the ion drift velocity (de la Beaujardière *et al.*, 1984). For the present study, ion drifts measured during the summer experiments have been analysed to obtain neutral winds at lower-thermospheric heights. This is done by solving the steady-state ion equation of motion appropriate for *E*-region heights for the neutral velocity using estimates of the ion-neutral collision frequency and the electric field obtained from *F*-region ion drifts. The neutral winds have been analysed to obtain mean values and tidal structures, as well as evidence of disturbances originating from magnetospheric activity. Of the 56 available experiments, 14 fell within the summer season defined as the period ± 45 days from summer solstice. These experiments are listed in the table 1, along with a description of the signal pulse and beam positions used. In addition, several measures of the level of geomagnetic activity for the interval of the experiment are provided.

As shown in table 1, the experiments were performed in several different modes. All approached or exceeded 24 h in duration and used three different fixed positions for the radar beam. The observations were carried out cyclically in three directions at elevation angles between 70 and 76.5°, and azimuths separated by 120°. Observation times were 3, 5, or 10 min per position, but typically the time interval was 5 min.

Vector ion velocities were derived assuming the vector velocity was the same at each position sampled, but the usual assumption that the vector was constant for the three observations was relaxed. Instead the line-of-sight velocities were allowed to vary linearly in time. To use this more realistic assumption, five line-

Table 1

Summer season

Date
760810-(
770518-(
77061
78051
7806(
780712-(
780801-(
790619-(
800514-(
800611-(
800708-(
800813-(
810513-(
810714-(

Definitions :

MP-3A	= 3
MP-3AE	= 3
S	= s
L	= l
$L(D)$	= l
$M(60)$	= r
$M(160)$	= r
$\sum K_p$	= s
$\overline{K_p}$	= (

of-sight mea
vector ion ve
$\mathbf{v}_\perp$. The obs
interpolated
When the ol
tion angles,
mon altitude
Above 180 l
quency is s
effectively c
perpendicula
$-\mathbf{v}_\perp \times \mathbf{B}$, al
from the *F*-r
vector veloc
were conver
magnetic fie
Division 1, V
altitude. For
reciprocal of
were within
mean. The
electric field
vector velo
analysis pro
field, and
derive the t
For steady

Table 1

Summer season Chatanika E-region experiments.

Date	Time (UT) start-end	Mode antenna	Pulse	A_p	$\sum K_p$	$\overline{K_p}$
760810-0811	2340-1026	MP-3A	*L*, *S*, *M*(160)	5	10	1+
770518-0519	0112-0951	MP-3A	*L*, *S*, *M*(160)	11	19+	2+
	1051-1144					
	1204-2025					
	2045-0114					
770616	0145-2400	MP-3A	*L*, *S*, *M*(160)	10	17-	2
780510	0001-0943	MP-3A	*L*, *S*, *M*(160)	10	13+	1+
	0958-1127					
	1141-1312					
	1327-1817					
	1835-2010					
780607	0001-2400	MP-3A	*L*, *S*, *M*(160)	11	20+	3-
780712-0713	2009-2008	MP-3A	*L*, *S*, *M*(160)	4	9	1
			L, *S*, *M*(60)	20	26-	3
780801-0802	2304-2313	MP-3A	*L*, *S*, *M*(160)	4	7	1-
790619-0620	2354-2359	MP-3A	*L*(*D*), *S*, *M*(160)	8	16-	2
800514-0515	0002-0001	MP-3A	*S*, *L*(*D*), *M*(60)	17	24+	3
800611-0612	0005-0004	MP-3A	*S*, *L*(*D*), *M*(60)	59	41+	5+
800708-0710	2358-0002	MP-3A	*S*, *L*(*D*), *M*(60)	8	16-	2
800813-0814	0007-1159	MP-3A	*S*, *L*(*D*), *M*(60)	6	12	1+
				6	12+	1+
810513-0514	0018-0001	MP-3AE	*S*, *L*(*D*), *M*(60)	10	16-	2
810714-0716	2200-0002	MP-3AE	*S*, *L*(*D*), *M*(60)	4	7-	1-

Definitions :

MP-3A = 3 fixed positions at the same elevation but different azimuth
MP-3AE = 3 fixed positions at different azimuth and elevation — here specifically one position up **B**
S = short pulse (60 μs)
L = long pulse (320 μs)
L(*D*) = long pulse sampled for density
M(60) = multipulse with a 60 μs pulse followed by a pattern of three 60 μs pulses
M(160) = multipulse with a 160 μs pulse followed by another 160 μs pulse
$\sum K_p$ = sum of K_p during the experiment
$\overline{K_p}$ = daily average of K_p or K_p averaged over experiment duration

of-sight measurements were combined to find the vector ion velocity perpendicular to the magnetic field $\mathbf{v}_\perp$. The observed velocities from two positions were interpolated to the time of the middle observation. When the observations were made at different elevation angles, the data were also interpolated to common altitudes.

Above 180 km, where the ion-neutral collision frequency is so small that the ions and neutrals are effectively decoupled, the ion equation of motion perpendicular to the magnetic field reduce to $\mathbf{E}_\perp = -\mathbf{v}_\perp \times \mathbf{B}$, allowing the electric field to be determined from the *F*-region ion drifts. Above this altitude, the vector velocities perpendicular to the magnetic field were converted to electric field, using the appropriate magnetic field model for the experiment date (IAGA Division 1, Working Group 1, 1986), and averaged in altitude. For the average, they were weighted by the reciprocal of their variance, and included only if they were within two standard deviations of the sample mean. The result was a very precise estimate of the electric field $\mathbf{E}_\perp$. In the lower thermosphere, these vector velocities were combined, in another new analysis program, with the electric field, magnetic field, and the ion-neutral collision frequencies to derive the best estimate of the neutral winds.

For steady state, in the presence of an electric field $\mathbf{E}_\perp$ and magnetic field **B**, the ion equation of motion is

$$e(\mathbf{E}_\perp + \mathbf{v}_\perp \times \mathbf{B}) + m_i\, \nu_{in}(\mathbf{u}_\perp - \mathbf{v}_\perp) = 0 \qquad (1)$$

where $\mathbf{v}_\perp$ is the ion velocity, m_i is the ion mass, ν_{in} is the ion-neutral collision frequency (summed over all the neutrals) and $\mathbf{u}_\perp$ is the neutral velocity. Solving for $\mathbf{u}_\perp$, the expression for the neutral wind is obtained,

$$\mathbf{u}_\perp = \mathbf{v}_\perp - \left(\frac{\Omega_i}{\nu_{in}}\right)(\mathbf{E}_\perp + \mathbf{v}_\perp \times \mathbf{B}), \qquad (2)$$

where $\Omega_i = eB/m_i$ is the ion gyrofrequency. The mean ion mass in the lower thermosphere is assumed to be 30.5 amu, which represents 75 % NO^+ and 25 % O_2^+. At altitudes above 150 km O^+ ions are also introduced into the data analysis. The ion-neutral collision frequencies for collisions of O^+, NO^+ and O_2^+ with O, N_2, and O_2 are calculated from the expressions in Schunk and Walker (1973), and neutral atmosphere temperatures and densities were obtained from the complete MSIS-83 (Hedin, 1983) model.

Throughout the calculations, from the line-of-sight velocities to the vector ion velocities and to the vector neutral winds, the uncertainties were fully propagated. Included in the error propagation calculations was a term to account for the sensitivity of the derived wind

to the neutral atmosphere. Below about 110 km, the ion-neutral collision frequencies are so great that the neutral wind uncertainty is essentially equal to the statistical uncertainty of the ion velocity. At higher altitudes the second term on the right-hand side of equation (2) becomes more important as the neutral densities decrease. Systematic departures of the neutral atmosphere from the MSIS-83 model would lead to systematic errors in the derived neutral wind that would increase with altitude. Because this is a statistical study, short-term variations would tend to average out. To determine the sensitivity of the derived wind to an error in the neutral atmosphere density, a 25 % uncertainty was assumed for the neutral atmosphere. The effects of this uncertainty on the wind is one reason the neutral wind derivation was limited to altitudes below 125 km. With more complete information on neutral atmosphere density and temperature, equation (2) could be used to higher altitudes.

Finally, the derived neutral wind is in geomagnetic coordinates. One component is horizontal toward magnetic east ; the other is toward magnetic north with the zenith angle given by the magnetic dip angle. For ease in comparing the results to other observations and published theoretical work, the results have been rotated into geographic coordinates. Vertical wind velocities were assumed to be small in comparison with horizontal wind velocities, such that the neutral wind component in the magnetic meridian u_y was assumed to be produced solely through horizontal winds u_m, or $u_y = u_m \sin I$, where I is the inclination of **B** from the local horizontal. The horizontal neutral wind in the geomagnetic meridian and the component towards geomagnetic east were then rotated into geographic coordinates by an amount equal to the declination of the geomagnetic field.

In the following section, the mean flow and tidal analyses performed on the neutral winds determined from the incoherent-scatter measurements are described. Results are then compared with previous observations of mean flows and tides at high-latitudes in the lower-thermosphere and to appropriate tidal modelling results. Next, the results of an analysis of the geomagnetic activity dependence of the neutral winds are presented and compared with previous observations of the high-latitude lower-thermospheric response to magnetospheric forcing. Finally, the Chatanika results are compared with modelling results obtained with the NCAR Thermospheric General Circulation Model (TGCM) for different levels of steady-state magnetospheric convection and particle precipitation.

MEAN FLOW AND TIDAL ANALYSIS

Figure 1 shows the weighted average neutral winds over half-hour intervals for all 14 experiments in geographic coordinates. The weighted average of all the N measurements falling within each half-hour bin was calculated using

$$\bar{x} = \frac{\sum_{i=1}^{N} (x_i/\sigma_i^2)}{\sum_{i=1}^{N} (1/\sigma_i^2)}, \qquad (3)$$

where x_i represents the individual measurements of neutral wind in the zonal (u_x, positive toward the east) and meridional (u_y, positive toward the north) directions. σ_i is the theoretical uncertainty of each velocity determined by propagating the uncertainties from the line-of-sight measurements and the average electric field through the calculations described above in the data analysis section. A preselection of measurements was made by excluding points with uncertainty greater that 75 m/s. The results show no significant differences

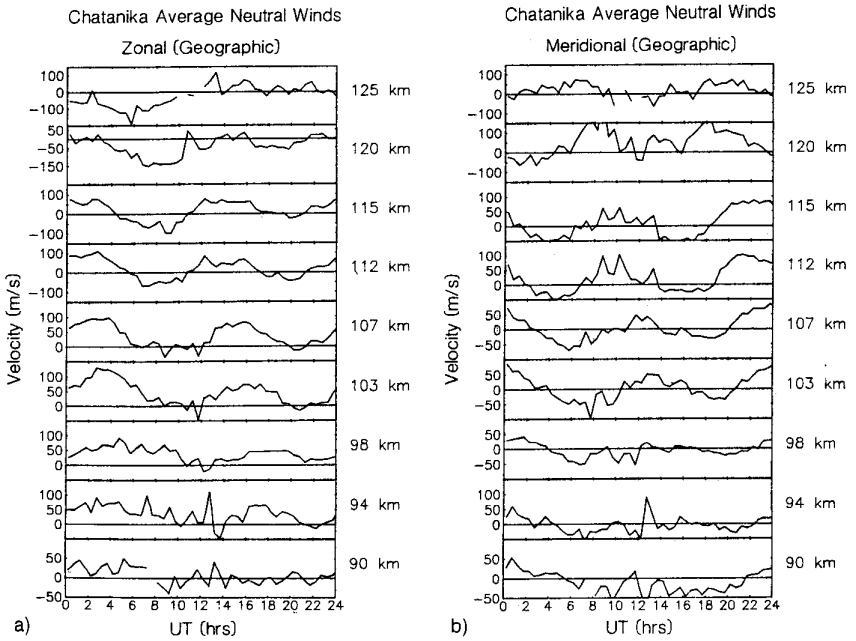

Figure 1
Weighted average zonal (a) and meridional (b) geographic neutral winds for all 14 *experiments. Each panel represents the average diurnal pattern observed at the altitudes specified at the right.* UT *in hours is given along the abscissa and is* 10 h *ahead of* LT *at Chatanika.*

from an unweighted average

$$\bar{x} = \frac{\sum_{i=1}^{N} x_i}{N}, \quad (4)$$

calculated without weighting by the uncertainty of each data point. The statistics are therefore sufficient that the average is not substantially skewed toward the 160 μs multipulse data, which has smaller uncertainty due to the longer pulse length and different data sampling scheme. The uncertainty of the mean, given by

$$\sigma_{\bar{x}} = \sqrt{\frac{\sigma^2}{N}}, \quad (5)$$

where σ^2 is the sample variance

$$\sigma^2 = \left(\frac{1}{N-1}\right)\left(\sum_{i=1}^{N} (x_i - \bar{x})^2\right), \quad (6)$$

has not been indicated on figure 1 and following figures in order to reduce complexity, however typical values range between 5 and 20 m/s. The 90, 98, 107, and 115 km averages had the best statistics, with ≈ 50 points per half-hour interval. These altitudes will be focused on in the discussions that follow.

The progression of a semidiurnal (12 h) oscillation through the panels in figure 1 covering the 90 to 125 km regime is obvious. At the highest altitudes, the zonal velocity is dominated by the diurnal component. Below that, the diurnal component is identified by a modulation of the semidiurnal oscillation, which apparently predominates at these lower heights. Mean flows are eastward between 90 and 115 km, and northward above 110 km.

Figures 2 through 4 present the results of the fit of a mean term together with a diurnal and a semidiurnal sine wave to the averaged zonal and meridional data (u_x and u_y) in the least-squares sense. The form used for the fit to each wind component separately was

$$u(t) = \alpha_0 + \alpha_1 \sin \omega t + \alpha_2 \cos \omega t + \alpha_3 \sin 2\,\omega t + \alpha_4 \cos 2\,\omega t, \quad (7)$$

where $\omega = (2\pi/24)\,\mathrm{h}^{-1}$. Here α_0 represents the average zonal or meridional wind over a diurnal cycle. The coefficients α_1 and α_2 are obtained from the fit of the diurnal sine wave, while the coefficients α_3 and α_4 result from the semidiurnal sine wave fit. Using the relations

$$A_0 = \alpha_0,$$
$$A_{24} = \sqrt{\alpha_1^2 + \alpha_2^2},$$
$$A_{12} = \sqrt{\alpha_3^2 + \alpha_4^2}, \; \phi_{24} = \tan^{-1}(\alpha_1/\alpha_2),$$

and $\phi_{12} = \tan^{-1}(\alpha_3/\alpha_4)$, where A_{24} and A_{12} are the amplitudes and ϕ_{24} and ϕ_{12} are the phases of the diurnal and semidiurnal oscillations, respectively, the equation for the fitting function can be rewritten as

$$u(t) = A_0 + A_{24} \cos(\omega t - \phi_{24}) + A_{12} \cos(2\,\omega t - \phi_{12}). \quad (8)$$

The phases presented in figures 3 and 4 represent the local time at which the eastward and northward excursions of the diurnal or semidiurnal oscillations maximized. The fit of equation (7) to the data has been weighted by the uncertainty of the mean for each half-hour interval, calculated using equations (5) and (6). The resultant uncertainties in amplitude and phase are indicated by the error bars in figures 2-4.

The results of these fits are compared with observations made at other high- and mid-latitude stations in tables 2 and 3 for 90 and 115 km, respectively, and are included for reference in the following sections. The previous results at Kiruna, Saskatoon, and Poker Flat were estimated from plots or taken from tables in the papers indicated.

Mean flows

In figure 2, a transition from eastward to westward flow in the lower thermosphere occurs between 115 and 120 km. The maximum eastward flow of about 50 m/s is reached near 100 km. A transition to westward flow below 90 km is indicated, at the interface with the upper mesosphere. Meridional mean flow changes from southward to northward at about 105 km as altitude increases.

Manson *et al.* (1985) have summarized the global mean wind distribution of the upper middle atmosphere to 110 km. The mean winds derived from the Poker Flat, Alaska (65° N) MST radar show that in the summer months the transition to eastward flows occurs between 88 km and 93 km (Carter and Balsley, 1982 ; Balsley and Riddle, 1984). Below this altitude a strong westward flow or « jet » is present. In addition, the mean meridional wind is southward above 85 km, with peak southward flows at the 95 km level. These same features are also displayed in the mean flows calculated using Poker Flat, MST meteor echoes (Tetenbaum *et al.*, 1986). However, both the MST meteor echo and the 1982 MST radar results (Manson *et al.*, 1985) show northward winds below 85 km, in contrast with the southward flows found below this height by Carter and Balsley (1982) and Balsley and Riddle (1984). The Poker Flat meteor radar data do not show an indication of flows turning northward above 100 km, as seen in the Chatanika data. Zonal winds measured at Kiruna, Sweden (68° N) are also eastward above 90 km during the summer months, and a westward jet is present below this height in the upper mesosphere. Mean zonal winds at Saskatoon (52° N) are eastward above 90 km during the summer months, turning strongly westward below this height. Meridional winds are southward between 80 and 98 km and are northward above this height. When the Chatanika mean winds are compared with the Saskatoon results for October 1979 to July 1980 (Manson *et al.*, 1981), the structures are very similar, although the altitude of transitions vary by a few km, and the amplitude of the peak zonal winds are about twice as high in the Chatanika data as in the Saskatoon data. Thus the Chatanika results are in overall good agreement with the comparable observations of mean winds at high latitude in the lower thermosphere.

The observations described above together indicate a

Table 2

Zonal and meridional mean winds and tidal components at 90 km.

Station	Zonal					Meridional				
	A_{0x} (m/s)	A_{24} (m/s)	ϕ_{24} (LT) (1)	A_{12} (m/s)	ϕ_{12} (LT)	A_{0y} (m/s)	A_{24} (m/s)	ϕ_{24} (LT)	A_{12} (m/s)	ϕ_{12} (LT)
Kiruna (2) (68° N, 20° E)										
8/74	27	8	0900	10	0500					
Chatanika (65° N, 147° W)										
Summer	7	15	1715	17	0720	− 13	27	1600	10	0330
Saskatoon (3) (52° N, 107° W)										
8/76	− 6	7	0500	14	0100	− 2	15	1700	12	0500
Saskatoon (4, 5)										
5/79		15	1900	14	0730			1300		0430
6/79		19	1900	15	0700			1530		0400
7/79		23	0300	18	0800			2000		0400
8/79		18	0730	14	0700			1030		0400
Saskatoon (6, 5)										
5/80	− 12	15	1600	22	0630	− 5		1400		0300
6/80	− 5	17	1900	18	0630	− 5		1520		0350
7/80	− 5	21	1920	19	0740	− 5		1230		0400
Poker Flat (7) (65° N, 147° W)										
Summer 79	− 13	28	2100	23	0700	− 18	20	1700	14	0400
Summer 80	− 28	16	0400	16	0800	− 18	18	1300	16	0400
Poker Flat (8)										
Summer 83	5	6	1600	8	0730	− 7	10	1200	9	0500
Summer 84		3	2200	8	0700		8	1200	8	0430

(1) Local time of maximum eastward or northward wind.
(2) Glass *et al.* (1978) ; results at 95 km.
(3) Stening *et al.* (1978).
(4) Manson *et al.* (1981).
(5) Amplitudes represent geometric mean of ellipse fit to both components.
(6) Manson *et al.* (1981).
(7) Carter and Balsley (1982).
(8) Tetenbaum *et al.* (1986).

Table 3

Zonal and meridional mean winds and tidal components at 115 km.

Station	Zonal					Meridional				
	A_{0x} (m/s)	A_{24} (m/s)	ϕ_{24} (LT) (1)	A_{12} (m/s)	ϕ_{12} (LT)	A_{0y} (m/s)	A_{24} (m/s)	ϕ_{24} (LT)	A_{12} (m/s)	ϕ_{12} (LT)
Chatanika (65° N, 147° W)										
Summer	14	29	1000	57	0345	7	21	1200	58	0000
Saskatoon (2, 3) (52° N, 107° W)										
5/79		23	0800	25	0500			1300		0200
6/79		26	1100	26	0530			1500		0400
7/79		30	1200	33	0630			2200		0400
8/79		27	1200	27	0630			1000		0330
Saskatoon (4, 3)										
5/80	5	18	1300	18	0445	7		1500		0400
6/80	3	21	1200	18	0445	3		0600		0400
7/80	7	23	1200	22	0600	7		0400		0430
Millstone Hill (5) (42° N, 71° W)										
Summer	3			33	0200	− 13			30	1100

(1) Local time of maximum eastward or northward wind.
(2) Manson *et al.* (1981).
(3) Amplitudes represent geometric mean of ellipse fit to both components.
(4) Manson *et al.* (1981).
(5) Wand (1983*a*) fit only semidiurnal oscillation on a seasonal basis.

Figure 2
Solid curves with meridional (b) g equation (7) *to obtained from the ble results obtain Balsley,* 1982), *w from the Saskatc Millstone Hill inc*

zonal mean w
about 90 and
below these l
meridional w
winds above a
summer-to-wi
the lower the
ture differenc
cold winter p

Figure 3
Same as figure 2 phase of zonal ((a) and (d)) velocitie (7) *to the data.*

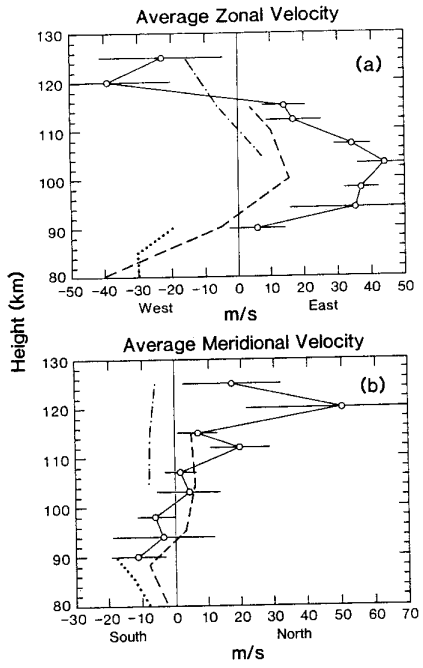

Figure 2
Solid curves with open circle symbols represent mean zonal (a) and meridional (b) geographic neutral velocities obtained from fit of equation (7) to the data. Error bars represent the uncertainty obtained from the least-squares fit. The dotted curve shows comparable results obtained with the Poker Flat, MST *radar (Carter and Balsley,* 1982*), while the dashed and dot-dashed curves show results from the Saskatoon partial reflection (Manson* et al., 1981*) and Millstone Hill incoherent scatter radars (Wand,* 1983*b*), *respectively.*

zonal mean wind profile with eastward flows between about 90 and 120 km, and westward winds above and below these heights. Between about 85 and 105 km, meridional winds are southward, with northward winds above and below. Roble *et al.* (1977) show that summer-to-winter meridional flow should develop in the lower thermosphere in response to the temperature difference between the hot summer pole and the cold winter pole, which is generated by solar EUV and UV heating. This meridional flow is deflected by the Coriolis force, resulting in a westward jet in the summer hemisphere. The same argument applies for the mesospheric circulation, where differential heating occurs during the summer months due to solar UV absorption by O_3. Thus a summer-to-winter meridional circulation is predicted in the summer mesosphere, which through Coriolis acceleration produces an intense westward jet (Holton, 1975).

The observations, on the other hand, clearly indicate an intervening region of eastward flow from 90 and 120 km where a solar driven circulation would predict westward flows. The work of Garcia and Solomon (1985) has shown that this reversal in the mean zonal flow results from breaking gravity waves, which decelerate the mesospheric jet. During summer months, the spectrum of upwardly propagating gravity waves from the lower atmosphere is effectively filtered by intervening stratospheric and mesospheric winds, allowing only eastward-travelling waves to reach upper-mesospheric heights (Lindzen, 1981). Through wave breaking, they deposit their eastward momentum to the mean flow. Southward meridional flows are generated in conjunction with this flow reversal, in agreement with the Chatanika observations below 105 km. The westward zonal winds at and above 115 km seen in the Chatanika data indicate a transition to the regime described by Roble *et al.* (1977), driven chiefly by UV absorption. Similarly, the indication of westward winds below 90 km presented here shows a change over to the regime described by Holton (1975).

Diurnal tide

Figure 3 shows the diurnal amplitude and phases for the zonal and meridional geographic neutral winds. Phase, as indicated before, is given as the local time of maximum eastward or northward wind in hours. The zonal diurnal component shows little change in amplitude with height below 110 km. Above this altitude, its amplitude dramatically increases from about

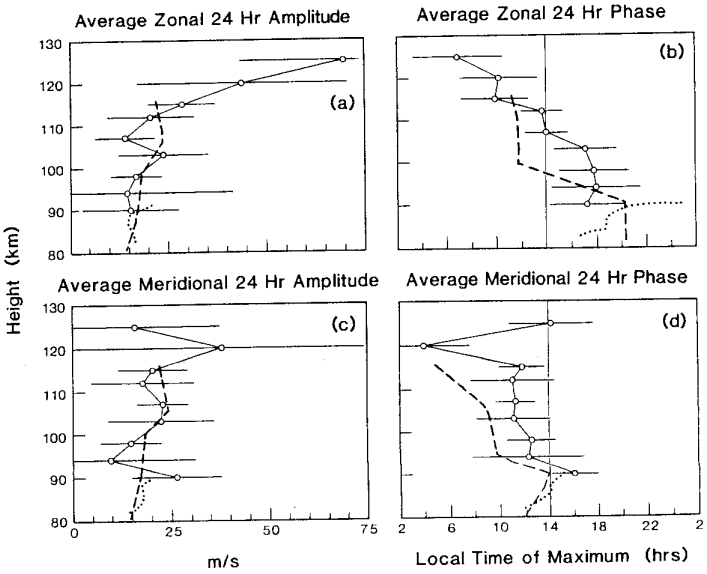

Figure 3
Same as figure 2 except diurnal amplitude and phase of zonal ((a) and (b)) and meridional ((c) and (d)) velocities obtained from fit of equation (7) to the data.

15 m/s to 25 m/s at 115 km and exceeds 50 m/s by 125 km. Similarly, the phase structure is apparently evanescent below 105 km, whereas above this height the phase shifts abruptly to earlier local times. The meridional component, on the other hand, shows no significant amplitude changes with height over the entire 90 to 125 km range, and its phase structure provides little evidence for a propagating tidal mode.

Forbes (1985) has summarized the observations of atmospheric tides between 80 and 120 km. The diurnal tide at high latitude is generally observed to be evanescent. The amplitudes and phases observed at Chatanika (tables 2, 3) are in reasonable agreement with those seen in the 1979 and 1980 results at Saskatoon and with those seen at Poker Flat at 90 km (Manson *et al.*, 1981*a*, *b* ; Carter and Balsley, 1982 ; Tetenbaum *et al.*, 1986). However, the phase of the zonal component at Kiruna and in the early Saskatoon results (Glass *et al.*, 1978 ; Stening *et al.*, 1978) are shifted toward earlier local time. In any case, the summary presented in table 2 shows that the diurnal tidal phase in both components is much more variable than the semidiurnal phase, in agreement with Forbes (1985). The shift in phase from later local times below 105 km to earlier local times above this, by about 8 to 10 h at 125 km for the zonal component, is paralleled by a shift in the later results at Saskatoon (Manson *et al.*, 1981) from a phase of about 20 local time (LT) at and below 90 km to about 12 LT at and above 100 km.

Forbes and Gillette (1982) have modelled the diurnal and semidiurnal tides for a realistic atmosphere from the surface to 400 km at equinox and December solstice. Their model includes the effects of mean winds and a realistic temperature distribution, including dissipative effects. They find that in the 90 to 150 km range, diurnal tidal oscillations are composed of nearly equal contributions from *in situ* excitation by UV and EUV absorption in the lower thermosphere and upwardly propagating components. At high-latitudes, the (1, 1) mode does not propagate. Below 100 km, the presence of the (1, – 2) evanescent mode is indicated by lack of phase progression and little change in amplitude with height. Although little phase progression is seen in the Chatanika diurnal component below 105 km, the amplitude profile found by Forbes and Gillette (1982) does not agree well with the Chatanika amplitudes reported here. At the lowest altitudes the Chatanika diurnal amplitudes are approximately twice as large as the model predicts, and the data do not indicate a peak amplitude at 110 km.

More recently, Forbes and Hagan (1986) have found that turbulent and molecular dissipation in the lower thermosphere and upper mesosphere lead to spreading of the upwardly propagating (1, 1) tidal oscillation to higher latitudes *via* coupling into the (1, – 2) and (1, – 1) evanescent modes. This mechanism, which was not included in the work by Forbes and Gillette (1982), is suggested to explain the relatively large amplitude diurnal oscillations found in the Poker Flat MST radar data (Carter and Balsley, 1982). In addition, dissipation leads to an amplitude peak for the lower-atmospheric diurnal oscillation at about 90 km. The evanescence and lack of increase in amplitude found for the diurnal tidal oscillation below 110 km is in good agreement with these theoretical results and suggests the presence of the (1, – 2) mode. The increase in amplitude of the zonal diurnal oscillation, and accompanying phase shift at and above 115 km, may be due to the growing influence of the *in situ* forced component in the lower thermosphere. The latter is from UV absorption, which peaks at about 110 km in the high-latitude summer hemisphere (Forbes and Gillette, 1982). Interestingly, the meridional component does not seem to show the same behavior.

Semidiurnal tide

The results of the semidiurnal component of the fit are shown in figure 4. The zonal and meridional components increase in amplitude from about 10 m/s at 90 km to over 60 m/s at about 115 km. Above this

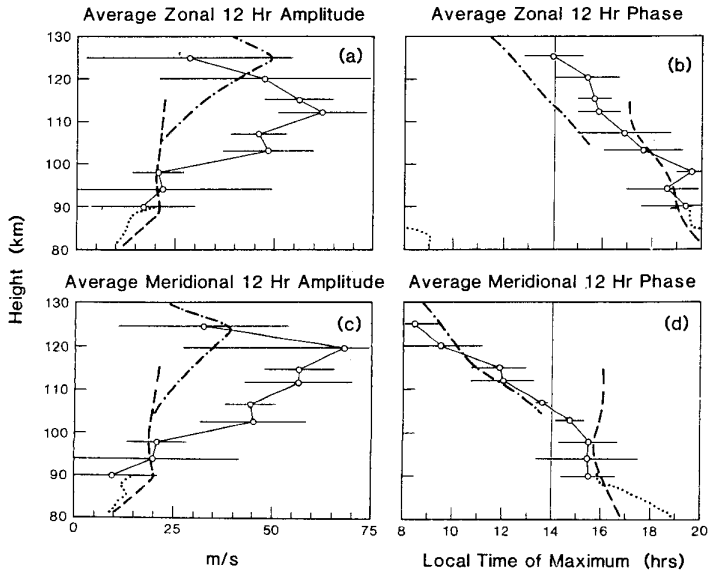

Figure 4
Same as figure 3 *except for the semidiurnal oscillation.*

height, both components decrease in amplitude, such that the zonal diurnal oscillation exceeds the semidiurnal, but the meridional semidiurnal appears to remain stronger than the meridional diurnal winds. The phase progression and the apparent quadrature between the two components is consistent with the presence of a propagating semidiurnal tidal oscillation. Quadrature is identified by comparing the local time of maximum meridional flow with that of the zonal flows — a consistent shift in phase of about 3 h, or 1/4 of the oscillation period, is evident. The phase progression of both components implies a vertical wavelength of about 50 km.

In an analysis of summer Poker Flat MST wind data, Carter and Balsley (1982) found a vertical wavelength for the semidiurnal oscillation of about 30 km. Their analysis yielded values for the zonal component phase of about 19.5 ± 2 h, and 16 ± 2 h for the meridional component at 90 km. Both components had amplitudes of about 15 m/s at 90 km. These results are in excellent agreement with those presented here, suggesting that the Chatanika data provide a smooth continuation to higher altitudes of observations made with the Poker Flat MST radar in the average sense.

At Kiruna, Glass *et al.* (1978) report summertime zonal amplitudes and phases of 10 m/s and 17 h LT at 95 km, also in good agreement with the results presented here. At lower latitudes, summertime vertical wavelengths of 100 km and more are usually observed (Forbes, 1985). At Saskatoon, semidiurnal tidal amplitudes of 15 to 20 m/s are seen throughout the 90 to 120 km altitude range with no indication of a decrease in amplitude above these heights. The vertical wavelengths indicated are substantially larger, from 90 to 140 km, although the phase at 90 km is only slightly later (about 1h) than it is at Chatanika. The Chatanika semidiurnal amplitude peak of about 65 m/s is more than three times greater than the comparable results at Saskatoon and may be due to differing contributions of the tidal modes as a result of the 10° latitude difference between the two stations.

Forbes *et al.* (1982) have modelled the effects of a realistic atmosphere with mean winds, temperature gradients, rotation and dissipation on the classical semidiurnal tidal modes. Due to these effects, Hough functions are no longer eigenfunctions of the governing equations in the thermosphere, and the resultant altered latitudinal structures are commonly described as « Hough Mode Extensions » (Hong and Lindzen, 1976). Comparison with the results of Forbes *et al.* (1982) at latitudes near 65° shows that the (2, 2), (2, 3), (2, 4), and (2, 5) modes all provide substantial contributions to the total semidiurnal oscillation. In addition, all 4 modes attain peak amplitudes within 10 km of one another near 110 km and have similar phase structures near the amplitude peaks. As a result, it is difficult to determine which semidiurnal tidal mode is chiefly responsible for the observed tidal structure. The vertical wavelength of the Chatanika semidiurnal tidal oscillation is about 50 km, which is closest to that of the (2, 4) mode found by Forbes *et al.* (1982). In addition, the peak amplitude for this mode occurs at about 110 km as well, in agreement with the observations. However, the other tidal modes all peak in this vicinity as well, and the observed vertical wavelength could undoubtedly result from a superposition of several different contributing modes.

Summary of tidal results

In general, the results presented here are in good agreement with the previously reported upper-mesospheric and lower-thermospheric observations at high latitude. The mean zonal wind profile is understood in terms of thermal circulations in the mesosphere and thermosphere, with the influence of gravity wave forcing at the mesosphere lower thermosphere interface. A rotation of the mean winds at Chatanika from south-eastward at 90 km in a counterclockwise sense to north-westward at 125 km occurs, as well as an increase in the mean flow velocities with altitude from about 15 m/s to 35 m/s. The diurnal tide is evanescent below 105 km and above that may show the influence of the *in situ* forced tide due to UV absorption. A strong propagating semidiurnal tidal oscillation is evident, with an amplitude peak of 65 m/s also at 110 km.

In figure 5, the pattern of neutral wind velocity variation with local time at 115 km caused by the diurnal, semidiurnal, and mean flow components is shown. The diurnal component (fig. 5*a*) produces a generally poleward flow from the dayside to the nightside in response to the temperature gradient resulting from solar heating. The semidiurnal wave (fig. 5*b*) produces a south-eastward flow near dawn and dusk, while poleward flows occur on the dayside and the nightside. The net tidal motion at 115 km due

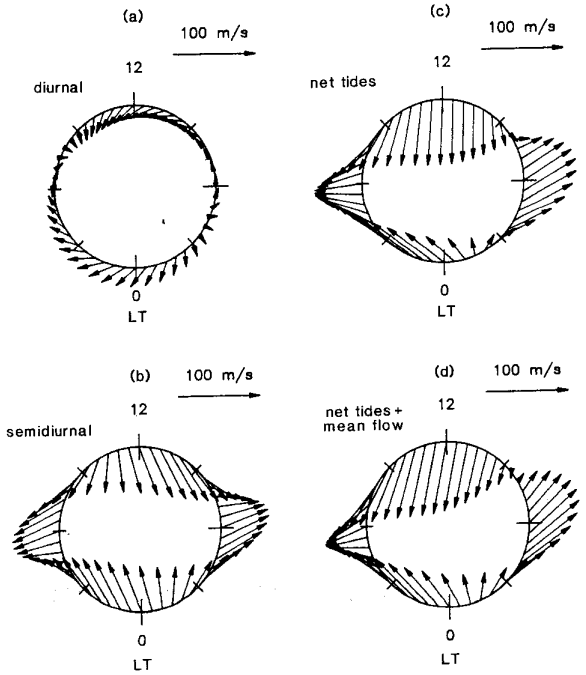

Figure 5
Polar plot showing the diurnal (a), semidiurnal (b), net tides (c), and tides plus mean flow (d) calculated from the least-squares fit to the average neutral wind velocity at 115 km. LT *is provided, along with a vector length scale.*

to both the diurnal and semidiurnal components is shown in figure 5*c*. The diurnal tide has enhanced the south-eastward flows from the semidiurnal component on the dawn side and opposed them at dusk. Finally, in figure 5*d*, the mean zonal and meridional flow has been added to the net tide shown in figure 5*c*. The net effect is strong south-eastward flow in the dawn sector, poleward and eastward flows across the dayside, shifting to equatorward flows near dusk. There, a transition from eastward to westward velocity results from the semidiurnal tidal component. In the midnight sector the net flow due to the combined mean flow and tidal components is poleward, produced dominantly by the semidiurnal component, shifting from the west to the east just after local midnight.

Tidal motions have been shown to be a dominant feature in lower-thermospheric neutral winds observed over Chatanika. With this appreciation of the magnitude and behavior of the tides in this data set, one can now attempt to properly assess the variability of the neutral winds caused by magnetospheric activity.

GEOMAGNETIC ACTIVITY EFFECTS

In the absence of Coriolis, pressure, inertia, and Hall-type ion drag forces, Pederson ion drag of convecting ions on the neutral gas acts to drive the neutrals to the same circulation as that of the ions. Ion drag provides an acceleration given by

$$\frac{\partial \mathbf{u}}{\partial t} = \frac{n_i}{n_n} \nu_{in}(\mathbf{v} - \mathbf{u}), \tag{9}$$

where $\mathbf{u}$ and $\mathbf{v}$ are the neutral and ion velocities, n_n and n_i are the neutral and ion number densities, and ν_{in} is the ion-neutral collision frequency. This provides a time scale of

$$\tau_{\text{drag}} = \frac{n_n}{n_i \nu_{in}} \tag{10}$$

(Baron and Wand, 1983) at which the neutral gas approaches the ion velocity following an instantaneous change in the ion drift (Killeen *et al.*, 1984). For the calculations presented here, based on the Schunk and Walker (1973) formulas for ν_{in} and the MSIS-83 neutral atmosphere the value $\nu_{in} \approx 4.1 \times 10^{-10} n_n \text{ s}^{-1}$ is typical. Thus $\tau_{\text{drag}} \approx 1/4.1 \times 10^{-10} n_i \text{ s}^{-1}$. Typical *E*-region ion number densities at 115 km above Chatanika range from $2 \times 10^4 \text{ cm}^{-3}$ or less for quiet nights to $1.5 \times 10^5 \text{ cm}^{-3}$ for quiet daytime conditions to $5 \times 10^5 \text{ cm}^{-3}$ or more during intervals of particle precipitation. Thus τ_{drag} can range from 38 h or more to less than 90 min, depending on the amount of ionization present. For typical active conditions in the data set, a time scale of ≈ 2 h is reasonable, and the neutral gas can be rather quickly driven to the motion of the ions. As activity decreases, the time scale for the neutrals to respond to the altered ion-convection pattern representative of quieter conditions lengthens. As a result, the neutrals are slow to adjust to the new ion circulation and continue to flow in the pattern driven by the ions under active conditions.

Ionospheric plasma drifts sunward in the auroral zone and anti-sunward over the polar cap at *F*-region heights in response to the ionospheric electric field imposed by magnetospheric convection. Thus the sense of ion drift is eastward in the morning sector and westward in the evening sector. As ν_{in} increases at lower altitudes, the ions develop a velocity component along $\mathbf{E}_\perp$, such that at *E*-region heights the ion drift vector has rotated clockwise by about 45° from the $\mathbf{E} \times \mathbf{B}$ drift direction (Roble *et al.*, 1982). The net sense of ion drift at these heights is therefore a south-eastward drift in the morning sector and a north-westward drift in the evening sector.

Heating of ions and neutrals occurs through Joule dissipation in regions where the ions and neutrals are in relative motion. The Joule heating rate can be expressed as

$$Q_J = \nu_{in} n_i m_i (\mathbf{u} - \mathbf{v})^2, \tag{11}$$

a form which makes its dependence on the velocity difference clear (Rino *et al.*, 1977). Incoherent scatter ion temperature enhancements due to Joule heating occur in the morning sector (Baron and Wand, 1983). Alcayde *et al.* (1984) have obtained similar results in a study of EISCAT observations. Thermospheric modelling has shown that Joule heating causes rising vertical motion of the heated atmosphere and is associated with a depletion of lighter constituents, such as O, and enhancement of heavier species, such as N_2 (Dickinson *et al.*, 1984 ; Roble *et al.*, 1984).

Previous results

A review of the literature on the response of the lower thermosphere to magnetospheric forcing shows that different researchers have obtained conflicting results. Table 4 provides a brief summary of some of these results, with response subdivided into four different local times centered on noon, dusk, midnight, and dawn. Some of these differences are undoubtedly due to the different techniques used by researchers. For instance, the meteor trail results of Hook (1970) average over the 75 to 110 km altitude range. Cogger *et al.* (1985) utilised the 5577 Å emission line of atomic oxygen to determine neutral winds at approximately 115 km with a Fabry-Pérot interferometer, however the altitude of the emission is not fixed, and in particular is sensitive to electron precipitation. Both of these techniques necessarily involve some averaging of the derived neutral winds over altitude. Similarly, Brekke *et al.* (1973, 1974) used a pulse scheme for the Chatanika radar which results in an *E*-region average neutral wind involving contributions from about 50 km centered on the gate in question. Finally, the results of Rees (1972), Heppner and Miller (1982) and Mikkelsen *et al.* (1981) all suffer from the lack of information about day-long time scale variations inherent in rocket release experiments. Wand (1983*a*) reported on incoherent scatter observations made by the Millstone Hill radar (42.6° N, 54.2° Λ) from July 1976 to November 1977 with 10 km altitude resolution, however these are not truely high-latitude results.

Examination of table 4 shows that in the evening and

Table 4

Lower thermosp

Hook (1970)	65° N meteor,
Rees (1972)	68° N rocket,
Brekke *et al.* (1	65° N Chatani
Brekke *et al.* (1	65° N Chatani
Rino *et al.* (197	65° N Chatani
Cogger *et al.* (1	60° N Fabry-P
Johnson (1987)	65° N Chatani
Heppner and M	
— 39 high-latitu	
— discontinuous	
Mikkelsen *et al.*	
— 2 65° N rock	
— non-pressure	
Wand (1983)	
— 46 days of 5	
— enhanced we	
— increased ne	

morning sectc
to increase i
activity. Two
the evening s
the morning s
One study fin
the early mor
high-resolutio
(1974) found
the dayside c
geomagnetic a
proton event.
less consisten
and equatorw
1974 ; Cogger
invokes high-
profiles of ne
experiments.]
hand, find th
during 39 high
with high-latit
The main dra
they did not c
tidal circulatic
neglect stemm
in the techniq
of data avail
based on the
field from th
global wind s

Table 4

Lower thermospheric wind changes attributed to magnetospheric forcing.

Investigator	Local time sector			
	Noon (0900-1500)	Evening (1500-2100)	Midnight (2100-0300)	Morning (0300-0900)
Hook (1970) 65° N meteor, 12/66-8/68			southward	
Rees (1972) 68° N rocket, 14 releases		west southward		east southward
Brekke *et al.* (1973) 65° N Chatanika,4 full, 2 partial days		west southward		east southward
Brekke *et al.* (1974) 65° N Chatanika, 3 full, 3 partial days, 8/3-9/1972	less poleward	southward	poleward	southward
Rino *et al.* (1977) 65° N Chatanika, 4 partial days		southward	poleward	poleward
Cogger *et al.* (1985) 60° N Fabry-Pérot, 75 nights			poleward and westward pre-midnight	southward
Johnson (1987) 65° N Chatanika, 14 full days	eastward	south-westward	westward turning eastward	eastward turning north to south
Heppner and Miller (1982) — 39 high-latitude rocket releases — discontinuous winds below 140 km inconsistent with high-latitude heating				
Mikkelsen *et al.* (1981) — 2 65° N rocket releases — non-pressure gradient flow implies high-latitude forcing				
Wand (1983) — 46 days of 56° N ISR results — enhanced westward mean wind, reduced semidiurnal amplitude and — increased neutral temperature				

morning sectors equatorward winds have been found to increase in response to enhanced geomagnetic activity. Two studies find enhanced westward winds in the evening sector and enhanced eastward winds in the morning sector (Rees, 1972 ; Brekke *et al.*, 1973). One study finds that poleward winds are enhanced in the early morning sector (Rino *et al.*, 1977), using the high-resolution Chatanika radar data. Brekke *et al.* (1974) found less-poleward directed neutral winds on the dayside during an interval of extremely active geomagnetic activity, coinciding with an intense solar proton event. In the midnight sector, the behavior is less consistent, with observations of both poleward and equatorward flows (Hook, 1970 ; Brekke *et al.*, 1974 ; Cogger *et al.*, 1985). Mikkelsen *et al.* (1981) invokes high-latitude forcing to explain the altitude profiles of neutral winds observed during two rocket experiments. Heppner and Miller (1982), on the other hand, find that the *E*-region wind profiles observed during 39 high-latitude rocket releases are inconsistent with high-latitude heating.

The main drawback of most of these studies is that they did not consider the normal lower-thermospheric tidal circulations to be expected in this region. This neglect stemmed largely from the limitations inherent in the techniques used, and from the limited amount of data available. Their conclusions were largely based on the deviations of the observed neutral wind field from the expected pressure gradient driven global wind system, which flows over the polar cap from the afternoon sector towards midnight. This can produce erroneous interpretations. In particular, it is important to note that the semidiurnal oscillation in the Chatanika *E*-region neutral winds at 115 km (see fig. 5*b*), which is largely the result of upwardly propagating tidal modes, produces equatorward winds turning from the east to the west at dusk as well as at 0800 LT, after dawn. Thus, the results obtained in previous studies described above may simply correspond to an observation of the normal semidiurnal oscillation expected for high-latitude neutral winds, and not to a response of the neutral winds to geomagnetic forcing. Brekke *et al.* (1973) point out this difficulty in separating tidal motions from the effects of ion drag at high-latitude. The Chatanika results presented here, on the other hand, explicitly consider the diurnal and semidiurnal tidal oscillations at lower-thermospheric heights. The 14 experiments presented, which greatly extend the number of *E*-region experiments at Chatanika described in the literature, have been analysed for typical quiet and active conditions, allowing differences due to increased activity to be determined.

Several studies, which did consider tidal effects, have suggested that geomagnetic activity results in changes in tidal modes observed in the lower thermosphere. Wand (1983*a*) found that mid-latitude neutral winds observed over Millstone Hill showed reduced semidiurnal tidal amplitudes during active intervals compared to quiet intervals. This was attributed to

either *in situ* generation of high-order semidiurnal oscillations possibly associated with auroral heating, or more likely to a change in the amount of dissipation in the lower thermosphere encountered by an upward-ly propagating tidal component. Rees (1979), in an analysis of a large data set consisting of mid-latitude rocket release observations, found that the diurnal (1, – 2) evanescent tidal mode was strongly enhanced following even mild geomagnetic activity.

Chatanika results

Averages

The experiments used in this study span the interval from 1976 to 1981, covering the rising and maximum phase of solar cycle 21. The level of geomagnetic activity during each experiment is indicated in table 1, where A_p, $\sum K_p$, and the mean value of K_p during the experiment $\overline{K_p}$ are provided. The 14 experiments are skewed towards lower activity levels, with only three days where $\overline{K_p}$ equaled or exceeded 3. In order to provide for the most equal distribution of experiments into activity levels, the days were divided into three groups for $\overline{K_p}$ less than, equal to, or greater than 2. The division by UT day is shown in table 5. Average neutral winds for each of the activity levels were calculated for each half-hour bin of UT.

Table 5

Division of Chatanika experiments by level of magnetic activity.

$\overline{K_p} < 2$	$\overline{K_p} = 2$	$\overline{K_p} > 2$
760810-0811	770616	770518-0519
780510	790619-0620	780607
780801-0802	800708-0710	780712-0713
800813-0814	810513-0514	800514-0514
810714-0716		800611-0612

Figure 6 compares average neutral winds for these different levels of activity at 90, 98, 107, and 115 km for the zonal (left) and meridional (right) components in geographic coordinates. Time is given along the abscissa in UT, which is 10 h ahead of UT at Chatanika. Uncertainties have not been indicated on these and following similar plots in order to reduce confusion. However, typical uncertainties for the mean range between 5 and 30 m/s during daylight

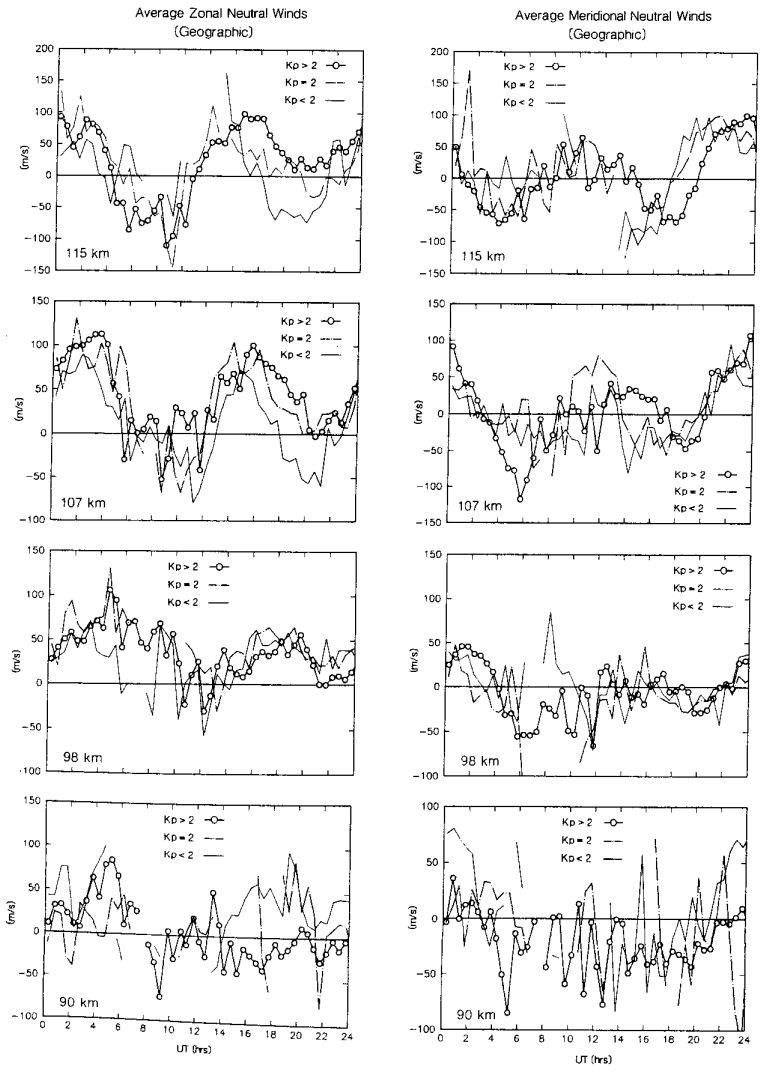

Figure 6

Average zonal (left) and meridional (right) neutral winds in geographic coordinates for quiet ($\overline{K_p} < 2$, solid curve), moderate ($\overline{K_p} = 2$, dot-dashed curve), and active ($\overline{K_p} > 2$, curve with open circles) geomagnetic conditions. Altitude is indicated in the lower left-hand corner of each plot.

hours, and incr
per bin.

Considering th
differences betv
and 98 km for
Although zonal
at 90 km in th
conditions, the
conditions are
lesser extent at
consistent differ
ing a progress
increases. At 1
developed enh
morning sector
the average fo
ment is even f
periments. At
LT sector is cor
the east durin
during the mos

The panels at t
the same ave
meridional cor
Consistent diffe
the meridional
the neutral wir
activity seems t
meridional com
consistent shift
90 km, the aver
statistics. At 9
more southwar
there are few
available for
meridional geo
the early morr
morning durin
hanced southwa
Figure 7 comp
and ion velocit
ward flow of th
poleward flowi
ward flow of th
equatorward fl

In figure 8, th
averaged neutr
obtained by sul
$K_p > 2$ average
115 (8*d*) km ha
plot format. A
eastward flow
south-eastward
mainly in the
poleward after
flows are enha
stronger towar
ocities are incr
and turn south-
similar to that
slightly later L
flows in the mic
flows after du
100 km (figs. 8

eater than 2.
le 5. Average
levels were

gnetic activity.

$\overline{K_p} > 2$
770518-0519
780607
780712-0713
300514-0514
300611-0612

ıds for these
, and 115 km
) components
en along the
l of UT at
indicated on
ler to reduce
ıties for the
ring daylight

eridional (right)
coordinates for
rve), moderate
e), and active
rcles) geomagne-
indicated in the
ach plot.

hours, and increase when fewer points are available per bin.

Considering the spread in the data, no substantial differences between the three curves are obvious at 90 and 98 km for the zonal geographic component. Although zonal winds are apparently more westward at 90 km in the local morning sector during active conditions, the statistics at this altitude for quiet conditions are particularly poor. This is also true to a lesser extent at 98 km. At higher altitudes, there are consistent differences among the three curves, indicating a progression of increasing effects as activity increases. At 107 and 115 km, the zonal component developed enhanced eastward flows in the local morning sector during the $K_p = 2$ intervals relative to the average for $K_p < 2$ experiments. This enhancement is even further developed for the $K_p > 2$ experiments. At 115 km, the zonal component in this LT sector is consistently about 80 m/s greater towards the east during the most active experiments than during the most quiet ones.

The panels at the right in figure 6 show the results of the same averaging performed on the neutral meridional component in geographic coordinates. Consistent differences are more difficult to discern for the meridional component. The strongest response in the neutral winds to different levels of geomagnetic activity seems to appear in the zonal component. The meridional component below 100 km does not show consistent shifts relative to the level of activity. At 90 km, the averages are particularly noisy due to poor statistics. At 98 km, although winds are apparently more southward during active intervals at local dusk, there are few points in the quiet time average available for comparison. At 107 and 115 km, meridional geographic winds are more northward in the early morning and more southward in the late morning during the most active experiments. Enhanced southward flows also occur near dusk (4 UT). Figure 7 compares geomagnetic meridional neutral and ion velocities at 115 km. The region of equatorward flow of the neutrals near dusk is coincident with poleward flowing ions. Similarly the region of poleward flow of the neutrals near dawn is coincident with equatorward flowing ions.

In figure 8, the difference between the half-hourly averaged neutral velocity in geographic coordinates obtained by subtracting the $K_p < 2$ average from the $K_p > 2$ average at 90 (fig. 8*a*), 98 (8*b*), 107 (8*c*), and 115 (8*d*) km has been plotted against LT in a polar plot format. At 115 km (fig. 8*d*), a pre-dawn north-eastward flow seems to continue into a post-dawn south-eastward flow. Pre-noon, flows are enhanced mainly in the eastward direction becoming more poleward after noon. After dusk, south-westward flows are enhanced. Pre-midnight, the zonal wind is stronger towards the west. At 107 km (fig. 8*c*), velocities are increased toward the north-east at dawn and turn south-east and finally eastward, in a pattern similar to that seen at 115 km but occurring at a slightly later LT. There are also enhanced poleward flows in the mid-afternoon and enhanced equatorward flows after dusk, as in the 115 km results. Below 100 km (figs. 8*b* and 8*a*), although differences in

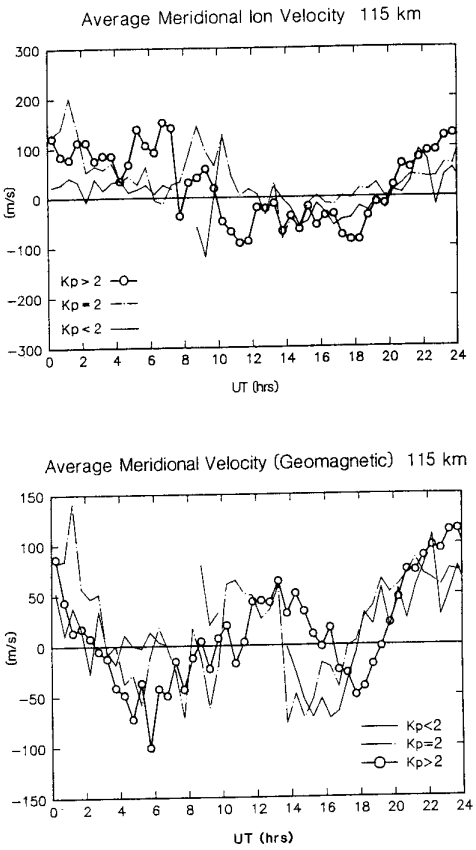

Figure 7
Meridional ion (top) and neutral (bottom) velocities in geomagnetic coordinates at 115 km.

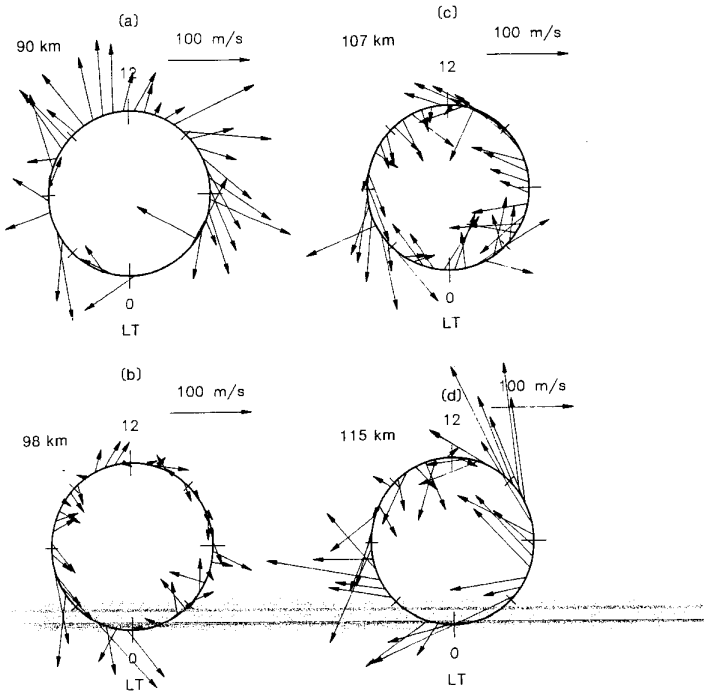

Figure 8
Local time polar plots of the difference between the averages calculated for the $K_p > 2$ *and* $K_p < 2$ *experiments at* 90 *(a),* 98 *(b),* 107 *(c), and* 115 *(d)* km. *A vector velocity scale is provided, and local midnight is indicated at* 0 LT.

excluding June 11, 1980, to check whether the enhanced eastward flows in the morning sector described above were simply the result of including this extreme day in the average. Similarly enhanced eastward zonal flows were obtained in the local morning sector even when it was excluded from the average.

The right-hand column of panels of figure 9 shows the same thing except for the meridional component at 115 km. The neutral flow is more southward during the entire morning sector, from 1200 to 2200 UT on June 11, 1980, than during the quietest experiments (bottom panel at right). Flow was more poleward after noon and was apparently stronger towards the south at dusk. In geomagnetic coordinates (center panel at right), the southward meridional flow after dusk is particularly evident. Meridional ion velocities (top panel at right), on the other hand, are strongly enhanced in the poleward direction from noon until just after dusk.

In figure 10, the difference between the June 11, 1980 neutral vector velocities and the average obtained for the $K_p < 2$ experiments in geographic coordinates at 90 (fig. 10*a*), 98 (10*b*), 107 (10*c*), and 115 (10*d*) km is shown on a·LT polar plot using the same format as figure 8. Notice that the vector velocity scale in plot (10*d*) is 200 m/s instead of the 100 m/s scale used in the other plots. Pre-midnight flows at 98 (fig. 10*b*), 107 (10*c*), and 115 (10*d*) km are increased towards the south during an initial milder burst of activity, with a westward component at 115 km. In the morning sector through noon, flows are very strongly enhanced toward the south-east at 115 km (fig. 10*d*) during a second and more intense interval of activity, to the extent that a reversal of the normal neutral circulation pattern in this sector has occurred. However, at 107 (fig. 10*c*) and 98 (10*b*) km, the increased eastward velocities during this interval are accompanied by a poleward component. When these polar plots are compared with those of figure 8, similar overall behavior is seen. However, at 107 km for June 11, 1980 (fig. 10*c*), the poleward flows seen in the afternoon and early morning sectors in figure 8*c* have been reversed, and instead enhanced equatorward flow is apparent. Additionally, at 98 km (fig. 10*b*), flows are increased towards the northeast after dawn until noon, while little ordered behavior is evident in the average results shown in figure 8*b*.

Figure 9 shows that ion velocities at 115 km on June 11, 1980 exceed neutral velocities an average of about 100 m/s in the local morning sector. This difference in velocities in the morning sector, in conjunction with the elevated conductivities observed during this interval, allows the ion-drag force to act as a momentum source for the neutral gas. The fact that the zonal neutral velocity already exceeds the normal zonal velocity by the order of 200 m/s in this LT sector towards the direction of ion flow indicates that the ion-drag force has already been effective in driving the neutral circulation towards that of the ions.

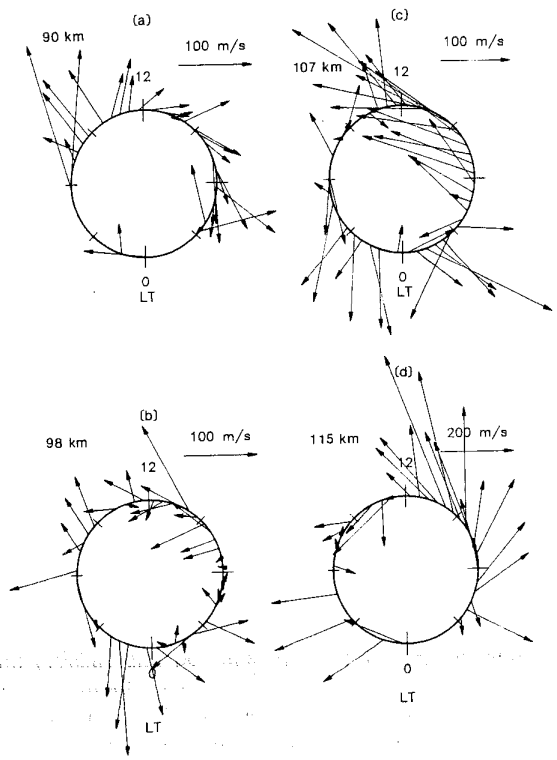

Figure 10

Same as figure 8 except for the difference between the June 11, 1980 and $K_p < 2$ experiments. Note that the velocity scale on the 115 km plot (d) is twice as large as that used for the other plots.

Discussion

In the Chatanika experiments studied here, which are averaged together on the basis of the level of activity, differences in tidal amplitudes are apparent. For instance, in figure 6 at 115 and 107 km, the $K_p < 2$ curve shows a larger amplitude semidiurnal fluctuation in both components than the $K_p > 2$ curve. Alternatively, the diurnal oscillation can be considered to be enhanced relative to the semidiurnal oscillation. This is most clearly seen on the most active day, June 11, 1980, when the zonal component and to some extent the meridional component display an almost purely diurnal fluctuation. The effect of ion drag on the neutral wind was evidently to accelerate the neutrals in the eastward and equatorward direction in the morning sector through collisional coupling to the convecting ions. This effectively reversed the normal flow direction in the morning to late morning sector, such that the second westward and northward excursions of the neutral winds due to the semidiurnal tide, which would normally occur during this LT sector, are absent. If a fit of a semidiurnal sine wave was done to these active data, the amplitude would, as a result, be substantially reduced compared to the quiet time amplitude.

These results display the same features identified by Wand (1983*a*) and perhaps by Rees (1979), as well. However, an alternative interpretation is offered. The variations in the tidal fluctuations observed in the Chatanika data are understandable purely on the basis of ion-drag coupling. Although geomagnetic activity may well affect the lower-thermospheric dissipation rate for upwardly propagating tidal components, either by altering the temperature dependent

coefficients of molecular viscosity and thermal conductivity, or by mean flow interactions, such mechanisms are not required to explain the Chatanika observations. The transitory nature of geomagnetic activity as well as the long set-up times of truely tidal oscillations (Bernard, 1981), implies that these changes are not the result of the generation of a diurnal tidal component. Instead, the apparent reduction in semidiurnal amplitude and enhancement in diurnal amplitude result from the relationship between the diurnal phase of ion-drag forcing and the semidiurnal phase of normal tidal motions. Ion-drag forcing produces a south-westward neutral wind component in the evening sector after dusk, during the same period that the usual semidiurnal oscillation is toward the south and turning from the east to the west. On the other hand, in the dawn sector, ion-drag forcing produces a south-eastward neutral wind component, during the same period that the normal semidiurnal oscillation is toward the south and turning from east to west. This results in enhancement of the evening sector semidiurnal oscillation and reduction of the morning sector oscillation, so that the resultant net oscillation is more diurnal than semidiurnal in character.

COMPARISON WITH THERMOSPHERIC GENERAL CIRCULATION MODEL RESULTS

During the past decade, two general circulation models of the thermosphere have been developed, one at the National Center for Atmospheric Research (NCAR) and one at University College London (UCL) in order to predict the response of the ionosphere-thermosphere system to magnetospheric forcing (Dickinson *et al.*, 1981 ; Fuller-Rowell and Rees, 1980). These models numerically solve the equations of energy, momentum, continuity, and state which describe neutral dynamics in their full and nonlinear form on a spherically nested grid and as a function of time.

Many studies have shown the good correspondence between *F*-region observations and modelling results from both of these models (Hernandez *et al.*, 1982 ; Rees *et al.*, 1983 ; Roble *et al.*, 1983 ; Hays *et al.*, 1984 ; Killeen *et al.*, 1984 ; Roble *et al.*, 1984 ; Hernandez and Roble, 1984 ; Emery *et al.*, 1985 ; Killeen *et al.*, 1986 ; Sica *et al.*, 1986). Only Fesen *et al.* (1986) made comparisons with lower-thermospheric wind observations, but these were obtained mainly from low- and mid-latitude stations. Both models predict substantial neutral temperature asymmetries and the production of strong long lasting vortex-like circulations accompanied by vertical upwelling in the lower thermosphere as a result of ion-drag momentum coupling and Joule heating (Roble *et al.*, 1982 ; Killeen and Roble, 1984 ; Fuller-Rowell and Rees, 1981). Some evidence of these changes should be apparent in the data and thermospheric modellers are anxious for such a comparison to be made. In order to provide this comparison, several runs of the NCAR TGCM were made for different levels of steady-state magnetospheric forcing and compared to average Chatanika neutral winds for the different levels of activity described above.

Details of the basic structure of the TGCM are provided in Dickinson *et al.* (1981). More recently, Dickinson *et al.* (1984) extended the model to include the coupling of thermospheric composition and dynamics. The TGCM allows the geographic and geomagnetic poles to be specified separately, and displaced poles are used in the results presented here. This produces a UT dependence of the thermospheric circulation pattern as a result of the rotation of the magnetic pole into and out of the illuminated hemisphere (Roble *et al.*, 1982). The Heelis ion convection model (Heelis *et al.*, 1982) is used to specify the global pattern of ionospheric convection as a function of latitude, longitude, potential difference and UT. The Chiu (1975) model of electron densities is used for calculation of ion-drag parameters, in conjunction with the MSIS-83 model of neutral temperature and composition (Hedin, 1983). In addition, the TGCM parameterizes the input of particle precipitation within the auroral oval (Roble *et al.*, 1986) using the discrete levels of particle precipitation specified by Foster *et al.* (1986).

Fesen *et al.* (1986) included upwardly propagating semidiurnal tidal components for equinox in the TGCM by forcing the lower boundary of the model (at 97 km) with the (2,2) and (2,4) semidiurnal geopotential height variations. The temperature and velocity fields at the lower boundary are determined from the Hough mode structure (Chapman and Lindzen, 1970). The amplitude and phase of the (2,2) and (2,4) geopotential height variations at the lower boundary is adjusted until agreement with incoherent scatter observations at higher altitude is obtained. Incoherent scatter data from Arecibo (18° N), Millstone Hill (43° N), and Saint-Santin (45° N) were used for this comparison. Results presented here included the equinox semidiurnal tides for solar maximum conditions (Fesen, private communication) in the absence of the solstice tidal parameterization. The phase of the semidiurnal oscillation included in the model runs agrees surprisingly well with the lower-thermospheric tidal variation seen at Chatanika, implying that the (2,2) and (2,4) modes are dominant even at solstice. As mentioned above, the semidiurnal tidal wavelength and altitude of amplitude maximum for the Chatanika data are consistent with the (2,4) mode (Forbes *et al.*, 1982). *In situ* generated semidiurnal and diurnal oscillations, due to UV and EUV absorption in the thermosphere and ion-neutral momentum coupling are already explicitly included in the model. Upwardly propagating diurnal oscillations do not penetrate into the lower thermosphere, except at equatorial latitudes, and are therefore not included in the model.

In many previous studies, the ion convection pattern used in TGCM runs was sun-aligned with a « Volland »-type structure (Roble *et al.*, 1982) in order to approximate average conditions in the absence of any better understanding of variations of the ion convection pattern to be expected as a function of the level of activity. In the analysis presented here, the average patterns of ion convection determined by

Foster *et al.* (
and for three
were simulate
which the H
patterns wer
patterns speci
rent precipita
the dawn an
seemed to b
demarcate th
drop was then
shown in the

Figure 11 sho
the Foster *et*
propriate for
shown in ma
Heelis *et al.* (
grid centered
the same scal

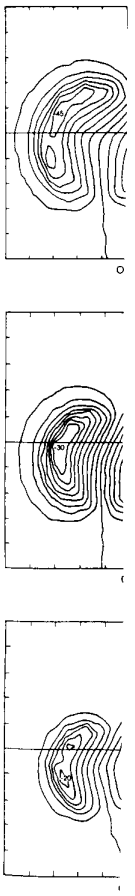

Geographic Loca

Figure 11
Comparison of t
Foster et al. (198
column), with ap
(1982) *ion convec*
(at the right) are
the approximatio
same scale on a
interval is indicat
plots at the left s
cells, and the thic
chosen to represe

Foster *et al.* (1986) using incoherent scatter radar data and for three different levels of particle precipitation were simulated by manipulating the parameters upon which the Heelis model is dependent until similar patterns were obtained. The Foster *et al.* (1986) patterns specify average potential drop for the different precipitation levels, but not its distribution over the dawn and dusk cells. Here, the contour which seemed to best bisect the two cells was chosen to demarcate the zero potential line, and the potential drop was then distributed as indicated by the contours shown in the Foster *et al.* (1986) results.

Figure 11 shows the result of this approximation of the Foster *et al.* (1986) ion convection patterns appropriate for levels 4, 7, and 9-10 (right column, shown in magnetic latitude/LT coordinates) with the Heelis *et al.* (1982) model (left column, shown on a grid centered on the geographic pole at 0000 UT), at the same scale. The zero potential lines chosen in the Foster *et al.* (1986) patterns are indicated by a thick contour on the plots at the right. The contour interval used for the plots at the left is 3 kV, while those at the right were provided with a 2 kV contour resolution. Although some small features of the Foster *et al.* (1986) patterns are not reproduced, for instance, the rotation of the potential contours for level 4 from sun-aligned to more nearly dawn-dusk aligned during the early morning between 70 and 80° invariant latitude, overall the simulation has been successful. Sharp features in the Heelis model approximations (left column) are due to the algorithm used in the NCAR contouring program used to generate these plots.

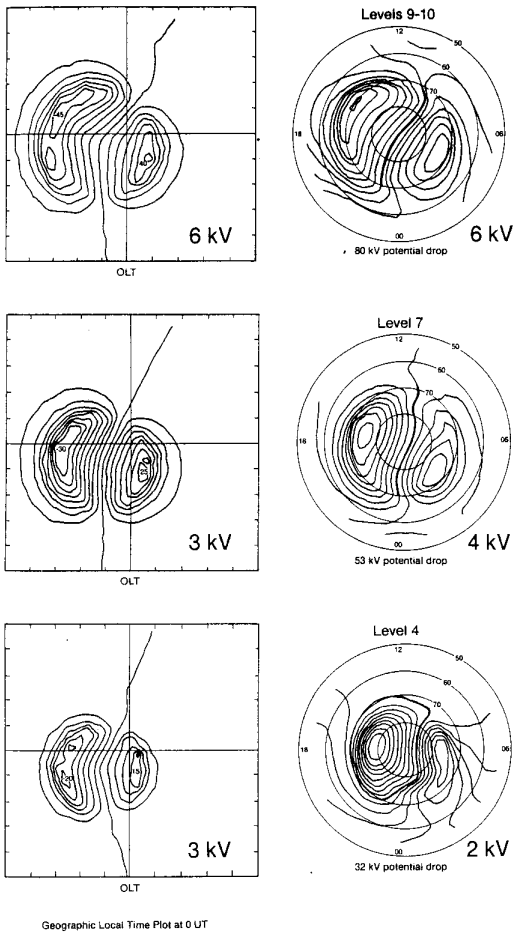

Figure 11

Comparison of the average ion convection patterns calculated by Foster et al. (1986) *for precipitation index levels* 4, 7, *and* 9-10 *(right column), with approximations to them made using the Heelis* et al. (1982) *ion convection model (left column). The Foster* et al. *patterns (at the right) are displayed in magnetic latitude/*LT *coordinates, while the approximations to these patterns (at the left) are displayed at the same scale on a grid centered on the geographic pole. The contour interval is indicated at the lower right of each plot. Numbers on the plots at the left show the potential extremes on the dawn and dusk cells, and the thick contour on the plots at right indicate the contour chosen to represent zero potential.*

A complex and global model such as the TGCM produces results in several different formats for many different chemical, dynamical and thermal parameters. This study concentrates on the dynamical predictions for the neutral circulations. Figures 12 through 13 show time history *versus* altitude contour plots of zonal and meridional neutral winds in geographic coordinates for the TGCM model runs described above. These composite figures show the model results at the Chatanika grid point (62.5° N and 145° W) from the lowest activity model run (precipitation index 4) along the bottom, from the moderate activity run (precipitation index 7) in the center and from the highest activity run (precipitation index 9-10) at the top. On each plot, pressure level coordinates (given by ln (p_0/p), where $p_0 = 50$ μPa) are provided on a linear scale at the left and altitude on a logarithmic scale in km at the right. The area of interest for this study, for comparison with the Chatanika data, is the bottom portion of each plot from the -7 to -4 pressure levels, which typically represents the 97 to 130 km altitude range. Dashed and solid contours represent negative and positive velocities in m/s, respectively.

The semidiurnal oscillation which is forced at the lower boundary is clearly dominant in the lower thermosphere, up to about 120 km for the zonal component (fig. 12) and to about 150 for the meridional component (fig. 13) under quiet activity conditions. Several changes in the zonal and meridional neutral winds as a result of increased magnetospheric activity are evident in figures 12 and 13. As the level of activity increases, the zonal winds increase in the local morning sector (i.e., the second westward excursion of the semidiurnal oscillation during the UT day, from ≈ 18-24 UT, is reduced or vanishes). Meridional winds become increasingly southward in the local morning sector (in the vicinity of 1800 UT), but at all other LT are increased toward the north. At local dusk (0400 UT), this is seen in a reduction of the southward velocities normally observed due to the semidiurnal oscillation. This is due to the increasing influence of a region of poleward flows which extends downward from the upper thermosphere as the level of activity increases.

Above about 130 km (≈ -4.0 level), the zonal and meridional circulations shift from dominance by the semidiurnal oscillation to the diurnal pattern driven in the upper thermosphere. As the level of activity increases, neutral wind velocities increase sharply with altitude producing very sharp gradients at the

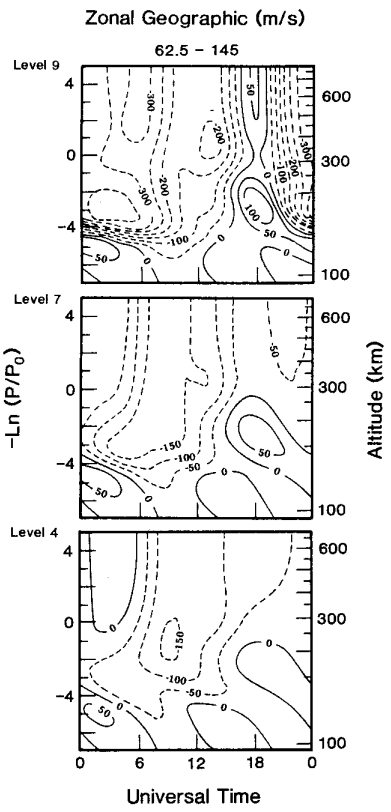

Figure 12

Composite plot of TGCM *neutral wind results in geographic coordinates for the three different levels of steady-state forcing. Each panel shows a contour plot of the time history of the zonal neutral wind in* m/s *at* 62.5° N *and* 145° W versus *altitude. The top plot shows the results for the highest activity run, corresponding to Foster* et al. (1986) *level* 9-10. *Similarly, the central and bottom plots display the results for the Foster* et al. (1986) *level* 7 *and level* 4 *runs, respectively. Positive zonal velocities are toward the east.*

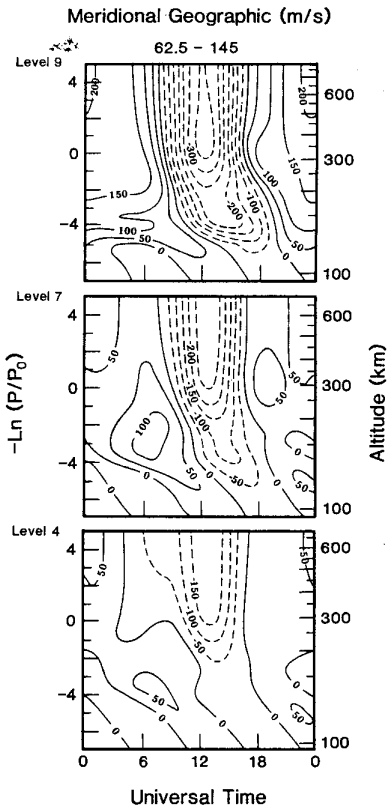

Figure 13

Same as figure 12 *except for the meridional component. Positive meridional velocities are toward the north.*

transition altitude. Results for the highest activity run give peak westward and southward winds at 130 km of about – 250 m/s. As the intensity of magnetospheric convection and particle precipitation increases, the altitude at which this transition from diurnal to semidiurnal tidal behavior occurs is lowered, such that the influence of magnetospheric forcing becomes progessively more dominant at lower altitudes as the forcing intensifies.

Figure 14 shows line plots of the TGCM model results for the $z = -5$ level, (≈ 115 km), for the zonal (above) and meridional (below) neutral winds in geographic coordinates. The solid, dashed, and open circle curves represent the results for Foster *et al.* (1986) levels 4, 7, and 9-10, respectively. These predictions are generally in good agreement with the observations at Chatanika. For easier comparison, figure 15 shows the same results presented in figure 6 at 115 km, but smoothed with a 3-h running average. Enhanced south-eastward flows were observed in the local morning sector, and this is also found in the model results. Model and observations both show that the eastward enhancement continues into the afternoon sector, where it turns poleward. Agreement with model results is also found before dawn, where both model and observations find increased poleward

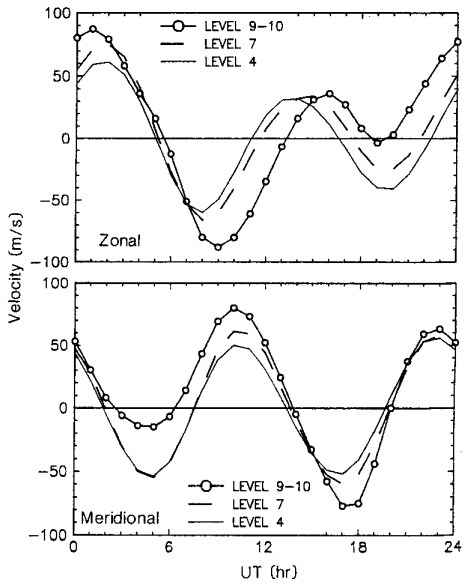

Figure 14

TGCM *model results for the zonal (top) and meridional (bottom) geographic neutral wind components at the* $z = -5$ *level* (≈ 115 km) *and* 62.5° N *for three different runs with magnetospheric forcing appropriate to the Foster* et al. (1986) *levels* 4 *(solid curves),* 7 *(dashed curves), and* 9-10 *(solid curves with open circle symbol).* UT *is indicated along the abscissa.*

flows. Howe
model occur
Chatanika a
the model
westward fl
slightly later

Model resul
sector, howe
seen at Ch
between 020
predict an i
other than th
tions at Cha
have attribut
sector to the
pointed out
premature si
the normal
creased geo
studies as w
finding equ
thermospher
indicate a re
part of the
increases, th
off at lowe
region of in

The reason
possibility i
semidiurnal
component

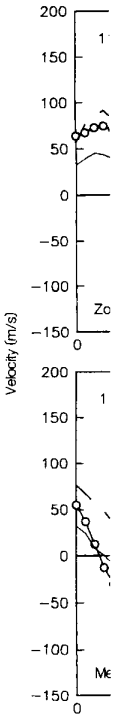

Figure 15

Average zonal coordinates for figure 6, *but sm*

flows. However, the enhanced poleward flows in the model occur at slightly earlier LT than they do in the Chatanika average results shown in figure 15. Both the model and the averaged data show increased westward flows after dusk, although this occurs at slightly later LT in the model results.

Model results and observations differ in the dusk sector, however. Enhanced equatorward flows were seen at Chatanika during active intervals (fig. 15 between 0200 and 0600 UT), while modelling results predict an increased poleward flow in all LT zones other than the early morning sector. Previous observations at Chatanika and elsewhere (described above) have attributed equatorward neutral winds in the dusk sector to the influence of auroral activity. It has been pointed out above that such an identification was premature since no attempt has been made to separate the normal tidal variation from effects due to increased geomagnetic activity. However, these earlier studies as well as the results presented here agree in finding equatorward flows at dusk in the lower thermosphere at Chatanika. The model results also indicate a region of equatorward flow near dusk as a part of the semidiurnal oscillation, but as activity increases, the equatorward flows are progressively cut off at lower and lower altitudes by a descending region of increased poleward flow.

The reason for this discrepancy is unclear. One possibility is that the vertical wavelength of the semidiurnal oscillation in the model for the meridional component is too short, so that the data indicates a longer lasting southward component. This does not explain the good agreement found elsewhere between the model tidal predictions and the Chatanika observations, however. Alternatively, the model may underestimate the amount of Joule heating which occurs in the dusk sector. This could explain the strong equatorward flows observed there during active intervals. Finally, the patterns of ion convection and auroral precipitation used in the model runs, which approximate the results of Foster *et al.* (1986), may inaccurately describe the magnetospheric input in the vicinity of the dusk convection cell.

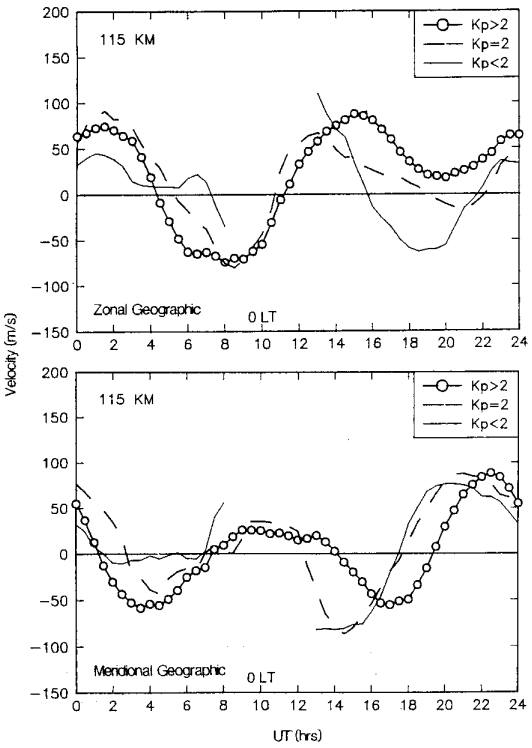

Figure 15

Average zonal (top) and meridional (bottom) winds in geographic coordinates for the three different K_p levels at 115 km *shown in figure* 6, *but smoothed with a* 3-h *running average.*

CONCLUSIONS

An analysis of summer *E*-region observations made by the Chatanika incoherent-scatter radar from 1976 to 1981 has been presented. Neutral winds at altitudes spanning the 90 to 125 km region have been derived from these observations, and the average flows and tidal structures have been studied. These results have been shown to be in good agreement with previous observations at mid- to high-latitude. The mean flows observed show the influence of deceleration of summer westward winds by gravity wave momentum deposition. Semidiurnal tides are quite strong and have a phase structure consistent with a propagating tide. Diurnal tides are not as strong as the semidiurnal until the highest altitudes are reached. The phase structure of the diurnal oscillation is consistent with an evanescent tidal mode, in agreement with modelling results.

The differences in the derived average neutral winds for three different levels of geomagnetic activity have been presented. At 115 km wind velocities are increased towards the north-east in the pre-dawn sector and toward the south-east in the post-dawn sector. This same pattern is evident at 107 km, shifted to slightly later LT. Poleward and eastward winds are also stronger at- and post-noon during geomagnetically active experiments. Increased south-westward flow was also observed after local dusk during these experiments at 115 km. The most active interval of the data set, June 11, 1980, showed these same characteristics at 107 and 115 km to a greater extent, with the exception that meridional flows were consistently more southward everywhere excluding the morning sector at 107 km. For this particular experiment, the effects of strong magnetospheric forcing are evident also at 98 km. Increased eastward and poleward flows develop in the pre-noon sector similar to those seen at 107 km, but are shifted slightly to later LT.

These changes in the neutral wind circulation during active intervals have been compared with the predictions of the NCAR Thermospheric General Circulation Model. The model was run for three different levels of steady-state magnetospheric convection and particle precipitation. In addition, the model runs included semidiurnal tidal forcing of the lower boundary. The tides calculated by the model in the lower thermosphere are in excellent agreement with the Chatanika tidal structures presented above. The dynamical changes found in the Chatanika lower-

thermospheric neutral winds described above are generally reproduced in the model results. One difference between model predictions and the data is found in the dusk sector, where model results predict increased poleward flow, while the data show increased equatorward flow. This difference may be due to an inadequate representation of the ion convection pattern in the dusk sector used for the model runs. In addition, the model may underestimate the level of Joule heating which occurs in this LT sector. In general, however, the degree of agreement between the model predictions and lower-thermospheric observations at Chatanika is quite encouraging.

Future studies will extend this analysis to the remaining 42 available *E*-region experiments conducted at Chatanika during other seasons of the 1976-1982 interval. In addition, neutral temperatures, which are also available using the incoherent-scatter technique, will be analysed for tidal components as well as changes related to geomagnetic activity.

Acknowledgements

The work presented here performed at UCLA was supported by NSF grant number ATM 85-15627. Research at SRI International was supported by NSF cooperative agreement ATM 85-16436. The authors would like to thank Carol Leger and Sam Todd for their assistance in the analysis and processing of the Chatanika radar data. The authors would also like to thank Barbara Emery and Ben Foster for their assistance in setting up and running the TGCM. Finally, we are grateful to Tim Killeen and Chris Tschan for providing us with a version of the Heelis model.

REFERENCES

Alcayde D., Bauer P., Fontanari J., 1984. Dynamical coupling of the auroral *F*-region ionosphere and thermosphere : Case studies. *J. Atmos. Terr. Phys.*, **46,** 625-633.

Amayenc P., 1974. Tidal oscillations of the meridional neutral wind at midlatitudes. *Radio Sci.*, **9,** 281-293.

Amayenc P., Reddy C. A., 1972. Height structure of tidal winds as inferred from incoherent scatter observations. *Planet. Space Sci.*, **20,** 1269-1279.

Aso T., Tsuda T., Takashima Y., Ito R., Kato S., 1980. Observations of lower ionospheric wind by the Kyoto meteor radar. *J. Geophys. Res.*, **85,** 177-184.

Balsley B. B., Riddle A. C., 1984. Monthly mean values of the mesospheric wind field over Poker Flat, Alaska. *J. Atmos. Sci.*, **41,** 2368-2375.

Banks P. M., Kockarts G., 1973. Aeronomy, Academic Press, New York, 220 pp.

Baron M. J., Wand R. H., 1983. *F*-region ion temperature enhancements resulting from Joule heating. *J. Geophys. Res.*, **88,** 4114-4118.

De la Beaujardière O., Wickwar V. B., Leger C. A., McCready M. A., Baron M. J., 1984. The software system for the Chatanika incoherent-scatter radar. Tech. Rep., 2nd ed., SRI Projects 4964 and 4995, SRI International, Menlo Park, CA, 127 pp.

Bernard R., 1974*a*. Tides in the *E*-region observed by incoherent scatter over Saint-Santin. *J. Atmos. Terr. Phys.*, **36,** 1105-1120.

Bernard R., 1974*b*. A comparison between meteoric radar and incoherent scatter measurements in the lower thermosphere. *Radio Sci.*, **9,** 295-300.

Bernard R., 1981. Variability of the semi-diurnal tide in the upper mesosphere. *J. Atmos. Terr. Phys.*, **43,** 663-674.

Brekke A., Doupnik J. R., Banks P. M., 1973. A preliminary study of the neutral wind in the auroral *E*-region. *J. Geophys. Res.*, **78,** 8235-8250.

Brekke A., Doupnik J. R., Banks P. M., 1974. Observations of neutral winds in the auroral *E*-region during the magnetospheric storm of August 3-9, 1972. *J. Geophys. Res.*, **79,** 2448-2456.

Carter D. A., Balsley B. B., 1982. The summer wind field between 80 and 93 km observed by the MST radar at Poker Flat, Alaska (65° N). *J. Atmos. Sci.*, **39,** 2905-2915.

Chapman S., Lindzen R. S., 1970. Atmospheric Tides, Thermal and Gravitational. D. Reidel Publ. Co., Dordrecht, Holland, 200 pp.

Chiu Y. T., 1975. An improved phenomenological model of ionospheric density. *J. Atmos. Terr. Phys.*, **37,** 1563-1570.

Cogger L. L., Murphree J. S., Tepley C. A., Meriwether J. W., Jr., 1985. Measurements of the *E*-region neutral wind field. *Planet. Space Sci.*, **33,** 373-379.

Comfort R. H., Wu S. T., Swenson G. R., 1976. An analysis of auroral *E*-region neutral winds based on incoherent scatter radar observations at Chatanika. *Planet. Space Sci.*, **24,** 541-560.

Dickinson R. E., Ridley E. C., Roble R. G., 1981. A three-dimensional general circulation model of the thermosphere. *J. Geophys. Res.*, **86,** 1499-1512.

Dickinson R. E., Ridley E. C., Roble R. G., 1984. Thermospheric general circulation with coupled dynamics and composition. *J. Atmos. Sci.*, **41,** 205-219.

Emery B. A., Roble R. G., Ridley E. C., Killeen T. L., Rees M. H., Winningham J. D., Carignan G. R., Hays P. B., Heelis R. A., Hanson W. B., Spencer N. W., Brace L. H., Sugiura M., 1985. Thermospheric and ionospheric structure of the southern hemisphere polar cap on October 21, 1981, as determined from Dynamics Explorer 2 satellite data. *J. Geophys. Res.*, **90,** 6553-6566.

Evans J. V., 1978. Incoherent scatter contributions to studies of the dynamics of the lower thermosphere. *Rev. Geophys. Space Phys.*, **16,** 195-216.

Fellous J. L. Bernard R., Glass M., Massebeuf M., Spizzichino A., 1975. A study of the variations of atmospheric tides in the meteor zone. *J. Atmos. Terr. Phys.*, **37,** 1511-1524.

Fesen C. G., Dickinson R. E., Roble R. G., 1986. Simulation of the thermospheric tides at equinox with the National Center for Atmospheric Research Thermospheric General Circulation Model. *J. Geophys. Res.*, **91,** 4471-4489.

Forbes J. M. 1985. Atmospheric tides between 80 km and 120 km. *Handbook for MAP*, **16,** 278-289.

Forbes J. M., Gillette D. F., 1982. A compendium of theoretical atmospheric tidal structures, part I : Model description and explicit structures due to realistic thermal and gravitational excitation. *Rep.* AFGL-TR-82-0173(I), Air Force Geophys. Lab., Hanscom AFB, Mass., 193 pp.

Forbes J. M., Hagan M. E., 1986. Diurnal propagating tide in the presence of mean winds and dissipation. *J. Geophys. Res.* (submitted).

Forbes J. M., Hagan M. E., DiCesare E., Gillette D. F., 1982. A compendium of theoretical atmospheric tidal structures, part II : Thermospheric extensions of the classical expansion functions for semidiurnal tides. *Rep.* AFGL-TR-82-0173(II). Air Force Geophys. Lab., Hanscom AFB, Mass., 153 pp.

Foster J. C., Holt J. M., Musgrove R. G., Evans D. S., 1986. Ionospheric convection associated with discrete levels of particle precipitation. *Geophys. Res. Lett.*, **13,** 656-659.

Fuller-Rowell T. J., Rees D., 1980. A three-dimensional time-dependent global model of the thermosphere. *J. Atmos. Sci.*, **37,** 2545-2567.

Fuller-Rowell T
dependent sim
thermosphere t
43, 701-721.

Garcia R. R.,
waves on the dy
and lower ther

Glass M., Spizz
Recent experir
1825-1839.

Glass M., Ber
French Meteor

Harper R. M.,
to-day variabilit

Hays P. B., Ki
R. G., Emery
Craven J. D.,
thermosphere.

Hedin A., 198
spectrometer a
Res., **88,** 1017(

Heelis R. A., L
latitude ionospl
6345.

Heppner J. P.,
latitudes from
1633-1647.

Hernandez G.,
heric winds an
the geomagnet
9049-9056.

Hernandez G.
Thermospheric
during two lar
Geophys. Res.

Holton J. R., 1
and Mesospher
Society, Lanca

Hong S. S., L
thermosphere.

Hook J. L., 19
Planet. Space

IAGA Division
tic reference fi

Killeen T. L.,
thermospheric
circulation mc
7509-7522.

Killeen T. L.,
W. B., Spence
the high-latitu
Dynamics Exp

Killeen T. L.
Meriwether J.
L. L., Sipler D
circulation in t
1649.

Lathuillere C.
scatter measu
temperatures i
Geophys. Res.

Lindzen R. S.,
and tidal breal

Manson A. H.,
wave motions
radiowave sou

Manson A. H.
atmospheric w
phere and lowe
the four seaso

Manson A. H.
waves (≈ 10 n
Saskatoon (52°
Space Sci., **29,**

Manson A. H.,
(10 min-30 day
Saskatoon (52°
to July 1980.

Fuller-Rowell T. J., Rees D., 1981. A three-dimensional, time-dependent simulation of the global dynamical response of the thermosphere to a geomagnetic substorm. *J. Atmos. Terr. Phys.*, **43,** 701-721.

Garcia R. R., Solomon S., 1985. The effect of breaking gravity waves on the dynamics and chemical composition of the mesosphere and lower thermosphere. *J. Geophys. Res.*, **90,** 3850-3868.

Glass M., Spizzichino A., 1974. Waves in the lower thermosphere : Recent experimental investigations. *J. Atmos. Terr. Phys.*, **36,** 1825-1839.

Glass M., Bernard R., Fellous J. L., Massebeuf M., 1978. The French Meteor radar facility. *J. Atmos. Terr. Phys.*, **40,** 923-931.

Harper R. M., 1981. Some results on mean tidal structure and day-to-day variability over Arecibo. *J. Atmos. Terr. Phys.*, **43,** 255-262.

Hays P. B., Killeen T. L., Spencer N. W., Wharton L. E., Roble R. G., Emery B. A., Fuller-Rowell T. J., Rees D., Frank L. A., Craven J. D., 1984. Observations of the dynamics of the polar thermosphere. *J. Geophys. Res.*, **89,** 5597-5612.

Hedin A., 1983. A revised thermospheric model based on mass spectrometer and incoherent scatter data : MSIS-83. *J. Geophys. Res.*, **88,** 10170-10188.

Heelis R. A., Lowell J. K., Spiro R. W., 1982. A model of the high-latitude ionospheric convection pattern. *J. Geophys. Res.*, **87,** 6339-6345.

Heppner J. P., Miller M. L., 1982. Thermospheric winds at high latitudes from chemical release observations. *J. Geophys. Res.*, **87,** 1633-1647.

Hernandez G., Roble R. G., 1984. Nighttime variation of thermospheric winds and temperatures over Fritz Peak Observatory during the geomagnetic storm of March 2, 1983. *J. Geophys. Res.*, **89,** 9049-9056.

Hernandez G., Roble R. G., Ridley E. C., Allen J. H., 1982. Thermospheric response observed over Fritz Peak, Colorado, during two large geomagnetic storms near solar cycle maximum. *J. Geophys. Res.*, **87,** 9181-9192.

Holton J. R., 1975. The Dynamic Meteorology of the Stratosphere and Mesosphere. *Meteorol. Monogr.*, **15,** American Meteorological Society, Lancaster Press, Lancaster, Pa., 218 pp.

Hong S. S., Lindzen R. S., 1976. Solar semidiurnal tide in the thermosphere. *J. Atmos. Sci.*, **33,** 135-153.

Hook J. L., 1970. Winds at the 75-100 km level at College, Alaska. *Planet. Space Sci.*, **18,** 1623-1638.

IAGA Division 1, Working Group 1, 1986. International geomagnetic reference field revision 1985. *EOS Trans. AGU*, **67,** 523-524.

Killeen T. L., Roble R. G., 1984. An analysis of the high-latitude thermospheric wind pattern calculated by a thermospheric general circulation model 1. Momentum forcing. *J. Geophys. Res.*, **89,** 7509-7522.

Killeen T. L., Hays P. B., Carignan G. R., Heelis R. A., Hanson W. B., Spencer N. W., Brace L. H., 1984. Ion-neutral coupling in the high-latitude *F*-region : Evaluation of ion heating terms from Dynamics Explorer 2. *J. Geophys. Res.*, **89,** 7495-7508.

Killeen T. L., Roble R. G., Smith R. W., Spencer N. W., Meriwether J. W., Jr., Rees D., Hernandez G., Hays P. B., Cogger L. L., Sipler D. P., Biondi M. A., Tepley C. A., 1986. Mean neutral circulation in the winter polar *F*-region. *J. Geophys. Res.*, **91,** 1633-1649.

Lathuillere C., Wickwar V. B., Kofman W., 1983. Incoherent scatter measurements of ion-neutral collision frequencies and temperatures in the lower thermosphere of the auroral region. *J. Geophys. Res.*, **88,** 10137-10144.

Lindzen R. S., 1981. Turbulence and stress owing to gravity wave and tidal breakdown. *J. Geophys. Res.*, **86,** 9707-9714.

Manson A. H., Gregory J. B., Stephenson D. G., 1974. Winds and wave motions to 110 km at mid-latitudes. I. Partial reflection radiowave soundings, 1972-1973. *J. Atmos. Sci.*, **31,** 2207-2215.

Manson A. H., Meed C. E., Stening R. J., 1979. The role of atmospheric waves (1.5 h-10 days) in the dynamics of the mesosphere and lower thermosphere at Saskatoon (52° N, 107° W) during the four seasons of 1976. *J. Atmos. Terr. Phys.*, **41,** 325-335.

Manson A. H., Gregory J. B., Meek C. E., 1981*a*. Atmospheric waves (≈ 10 min-30 days) in the mesosphere and thermosphere at Saskatoon (52° N, 107° W), October 1978-September 1979. *Planet. Space Sci.*, **29,** 615-625.

Manson A. H., Meek C. E., Gregory J. B., 1981*b*. Winds and waves (10 min-30 days) in the mesosphere and lower thermosphere at Saskatoon (52° N, 107° W, *L* = 4.3) during the year, October 1979 to July 1980. *J. Geophys. Res.*, **86,** 9615-9625.

Manson A. H., Meek C. E., Massebeuf M., Fellous J. L., Elford W. G., Vincent R. A., Craig R. L., Roper R. G., Avery S., Balsley B. B., Fraser G. J., Smith M. J., Clark R. R., Kato S., Tsuda T., Ebel A., 1985. Mean winds of the upper middle atmosphere (60-110 km) : A global distribution from radar systems (MF, meteor, VHF). *Handbook for MAP*, **16,** 239-253.

Massebeuf M., Bernard R., Fellous J. L., Glass M., 1981. Simultaneous meteor radar observations at Monpazier (France, 44° N) and Punta Borinquen (Puerto Rico, 18° N). II. Mean zonal wind and long period waves. *J. Atmos. Terr. Phys.*, **43,** 535-542.

Mathews J. D., 1976. Measurements of the diurnal tides in the 80- to 100-km altitude range at Arecibo. *J. Geophys. Res.*, **81,** 4671-4677.

Mathews J. D., Sulzer M. P., Tepley C. A., Bernard R., Fellous J. L., Glass M., Massebeuf M., Ganguly S., Harper R. M., Behnke R. A., Walker J. C. G., 1981. A comparison between Thomson scatter and meteor radar wind measurements in the 65-105 km altitude region at Arecibo. *Planet. Space Sci.*, **29,** 341-348.

Mikkelsen I. S., Jørgensen T. S., Kelley M. C., Larsen M. F., Pereira E., Vickrey J., 1981. Neutral winds and electric fields in the dusk auroral oval. 1. Measurements. *J. Geophys. Res.*, **86,** 1513-1524.

Müller H. G., 1966. Atmospheric tides in the meteor zone. *Planet. Space Sci.*, **14,** 1253-1272.

Pereira E., Kelley M. C., Rees D., Mikkelsen I. S., Jørgensen T. S., Fuller-Rowell T. J., 1980. Observations of neutral wind profiles between 115- and 175-km altitude in the dayside auroral oval. *J. Geophys. Res.*, **85,** 2935-2940.

Rees D., 1972. Winds and temperatures in the auroral zone and their relations to geomagnetic activity. *Phil. Trans. Roy. Soc. Lond. A.*, **271,** 563-575.

Rees D., 1979. Rocket measurements of annual mean prevailing diurnal and semi-diurnal winds in the lower thermosphere at midlatitudes. *J. Geomag. Geoelectr.*, **31,** 253-265.

Rees D., Carlson M., Maynard N. C., Kaila K. U., 1981. Neutral wind and electric field measurements in the upper mesosphere and lower thermosphere by chemical trial and rocket probe techniques. (Unpublished manuscript).

Rees D., Fuller-Rowell T. J., Gordon R., Killeen T. L., Hays P. B., Wharton L., Spencer N. W., 1983. A comparison of wind observations of the upper thermosphere from the Dynamics Explorer satellite with the predictions of a global time-dependent model. *Planet. Space Sci.*, **31,** 1299-1314.

Rino C. L., Brekke A., Baron M. J., 1977. High-resolution auroral zone *E*-region neutral wind and current measurements by incoherent scatter radar. *J. Geophys. Res.*, **82,** 2295-2304.

Roble R. G., Dickinson R. E., Ridley E. C., 1977. Seasonal and solar cycle variations of the zonal mean circulation in the thermosphere. *J. Geophys. Res.*, **82,** 5493-5504.

Roble R. G., Dickinson R. E., Ridley E. C., 1982. Global circulation and temperature structure of thermosphere with high-latitude plasma convection. *J. Geophys. Res.*, **87,** 1599-1614.

Roble R. G., Ridley E. C., Dickinson R. E., 1986. An auroral model for the NCAR Thermospheric General Circulation Model. *J. Geophys. Res.* (submitted).

Roble R. G., Dickinson R. E., Ridley E. C., Emery B. A., Hays P. B., Killeen T. L., Spencer N. W., 1983. The high latitude circulation and temperature structure of the thermosphere near solstice. *Planet. Space Sci.*, **31,** 1479-1499.

Roble R. G., Emery B. A., Dickinson R. E., Ridley E. C., Killeen T. L., Hays P. B., Carignan G. R., Spencer N. W., 1984. Thermospheric circulation, temperature, and compositional structure of the southern hemisphere polar cap during October-November 1981. *J. Geophys. Res.*, **89,** 9057-9068.

Schunk R. W., Walker J. C. G., 1973. Theoretical ion densities in the lower ionosphere. *Planet. Space Sci.*, **21,** 1875-1896.

Sica R. J., Rees M. H., Romick G. J., Hernandez G., Roble R. G., 1986. Auroral zone thermospheric dynamics, 1. Averages. *J. Geophys. Res.*, **91,** 3231-3244.

Solar-Geophysical Data, US Department of Commerce, Boulder, Colorado.

October 1976, **386,** Part I, p. 104.
July 1977*a*, **395,** Part I, p. 115.
August 1977*b*, **396,** Part I, p. 111.
July 1978*a*, **407,** Part I, p. 160.
August 1978*b*, **408,** Part I, p. 160.
September 1978*c*, **409,** Part I, p. 135.
October 1978*d*, **410,** Part I, p. 153.

August 1979, **420,** Part I, p. 160.
July 1980*a*, **431,** Part I, p. 151.
August 1980*b*, **432,** Part I, p. 158.
September 1980*c*, **433,** Part I, p. 150.
October 1980*d*, **434,** Part I, p. 147.
July 1981*a*, **443,** Part I, p. 144.
September 1981*b*, **445,** Part I, p. 160.

Stening R. J., Meek C. E., Manson A. H., Stephenson D. G., 1978. Winds and wave motions to 110 km at midlatitudes. VI. Tidal, gravity and planetary waves, 1976. *J. Atmos. Sci.*, **35,** 2194-2204.

Tetenbaum D., Avery S. K., Riddle A. C., 1986. Observations of mean winds and tides in the upper mesosphere during 1980-1984, using the Poker Flat, MST radar as a meteor radar. *J. Geophys. Res.*, **91,** 14539-14555.

Vincent R. A., Stubbs T. J., 1977. A study of motions in the winter mesosphere using the partial reflection drift technique. *Planet. Space Sci.*, **25,** 441-455.

Wand R. H., 1983*a*. Geomagnetic activity effects on semidiurnal winds in the lower thermosphere. *J. Geophys. Res.*, **88,** 9243-9248.

Wand R. H., 1983*b*. Seasonal variations of lower thermospheric winds from the Millstone Hill incoherent scatter radar. *J. Geophys. Res.*, **88,** 9227-9241.